Discover Computing

RESEARCH Open Access

A modular transcriptomic signature paired with machine learning reveals core immune pathways in sepsis diagnosis

Tanya Johari[1,2] and Davide Chicco[2,3*]

*Correspondence:
Davide Chicco
davide.chicco@unimib.it
[1]Dipartimento di Biologia e Biotecnologie, Università di Pavia, Pavia, Italy
[2]Dipartimento di Informatica Sistemistica e Comunicazione, Università di Milano-Bicocca, Milan, Italy
[3]Institute of Health Policy Management and Evaluation, University of Toronto, Toronto, Canada

Abstract

Sepsis remains a leading cause of mortality worldwide, with one in five deaths attributed to its rapid and heterogeneous progression. Early diagnosis is hindered by the absence of reliable molecular biomarkers. To address this, we developed an integrative computational framework that combines supervised machine learning, statistical testing, and cross-dataset reproducibility analysis to identify robust transcriptomic signatures of sepsis. From 55 experimentally validated sepsis-related genes curated from the literature, our pipeline selected a 15-gene diagnostic panel achieving consistent high performance across 11 independent gene expression omnibus datasets (Matthews Correlation Coefficient = 0.94; AUROC = 0.99). Feature ranking revealed four key predictors (CD177, S100A12, S100A8, and GATA3) that were repeatedly prioritized across independent datasets. Functional enrichment and network analysis further organized these genes into three coherent biological modules associated with neutrophil activation, immune suppression, and calgranulin-mediated inflammatory signaling. Benchmarking against established clinical panels confirmed superior accuracy, reproducibility, and interpretability. This study provides a reproducible, data-driven framework for biomarker discovery and a biologically grounded 15-gene panel for precision diagnostics in sepsis.

Keywords Sepsis, Gene expression, Machine learning, Random forest, Feature importance, Transcriptomics, Biomarker discovery, Pathway enrichment

1 Introduction

Sepsis is a severe clinical syndrome characterized by a dysregulated immune response to infection, rapidly leading to systemic inflammation, organ dysfunction, and potentially death. Triggered by diverse infectious agents, including bacteria, viruses, fungi, and parasites, sepsis remains a critical global health challenge, responsible for significant morbidity, mortality, and high healthcare expenditure worldwide [1]. High-risk groups include neonates, older adults, immunocompromised individuals, and patients with chronic illnesses such as diabetes or cancer [2].

The clinical progression of sepsis is driven by a complex interplay between pro-inflammatory and anti-inflammatory pathways. In the early stages, an excessive inflammatory response causes a surge of cytokines, commonly referred to as a "cytokine storm," which, while aimed at pathogen clearance, simultaneously causes collateral tissue damage. This response disrupts endothelial integrity, increasing vascular permeability and leading to widespread vascular leakage, tissue hypoxia, and impaired oxygen delivery. These processes contribute to microvascular thrombosis and multiorgan dysfunction, affecting the cardiovascular, renal, hepatic, neuronal, hormonal, and coagulation systems [3].

As the condition progresses, the immune response often shifts toward immunosuppression. This phase is marked by profound lymphocyte depletion, impaired antigen presentation, and suppressed cytokine production, rendering patients highly vulnerable to secondary infections [4, 5]. Survivors often face long-term complications such as fatigue, cognitive impairment, and psychological distress, which reduce quality of life and increase healthcare burden [6, 7].

Given that each hour of delayed treatment increases sepsis mortality by approximately 8% [8], rapid and accurate diagnosis is essential for improving patient outcomes. However, current diagnostic approaches face major limitations. Commonly used biomarkers, such as C-reactive protein (CRP) and procalcitonin (PCT), suffer from limited specificity, while gold-standard methods like blood cultures are time-consuming and often yield inconclusive results [9]. The nonspecific and heterogeneous nature of early sepsis symptoms further complicates timely recognition. These clinical challenges underscore the need for novel diagnostic strategies that are both biologically informed and clinically actionable.

Transcriptomic profiling offers a promising alternative by capturing host-derived gene expression signatures that reflect sepsis pathophysiology [10]. Despite the diagnostic promise of transcriptomic profiling, prior studies have been hampered by inconsistent definitions of sepsis and variable reproducibility across cohorts. A recent scoping review of transcriptomic studies in sepsis underscored the growing interest in gene expression-based biomarkers while also highlighting challenges such as inconsistent terminology, lack of reproducibility, and poor alignment between transcriptomic findings and clinical endpoints [11]. These limitations emphasize the need for standardized, biologically grounded approaches to biomarker discovery.

Beyond transcriptomics, Recent advances in biomarker discovery have increasingly embraced multi-omics integration and systems-level machine learning frameworks [12]. Numerous studies demonstrate the versatility of machine learning across diverse biomedical modalities, their approaches differ substantially in data type, clinical context, and methodological focus. For example, Noor et al. [13] developed an XGBoost-based pipeline to classify liver disease using demographic variables and routine laboratory values. Their workflow incorporated filter-based feature selection (Chi-square and ANOVA F-score), dimensionality reduction (PCA and LDA), and Fisher Score ranking to derive an optimized feature set. Almusallam et al. [14] designed a deep learning model to predict RNA 5-methyluridine (m^5U) modification sites, integrating hybrid sequence encodings and SHAP-based interpretability. Similarly, Khan et al. [15] introduced DeepProBind, a transformer-driven model that leverages protein sequence and structural features to identify binding peptides.

While all studies illustrate the strength of machine learning combined with targeted feature engineering, This study presents a reproducibility-focused framework for identifying transcriptomic biomarkers in sepsis, grounded in experimentally curated immune-related genes. We curated a panel of 55 genes previously validated in sepsis studies and assessed their diagnostic relevance across 11 independent, clinically annotated transcriptomic datasets. The analytical pipeline integrates statistical testing, Random Forest-based feature importance ranking, and correlation filtering to select robust gene markers. To support biological interpretability, selected features were further evaluated using pathway enrichment and protein–protein interaction analyses. This design draws inspiration from ensemble-based strategies that identify reproducible gene signatures across diseases using multi-cohort transcriptomic data [16, 17]. Benchmarking against established transcriptomic signatures confirmed superior diagnostic performance and clearer mechanistic relevance. This integrative and multi-cohort strategy provides a scalable foundation for translational biomarker discovery in sepsis and related immune disorders.

2 Data and methods

2.1 Gene selection and literature review

We curated a panel of genes implicated in sepsis pathophysiology through an extensive review of the biomedical literature (step *a* in Fig. 1), prioritizing those repeatedly validated across independent clinical or experimental cohorts. To minimize study-specific bias during the literature curation stage, genes were included only if they were

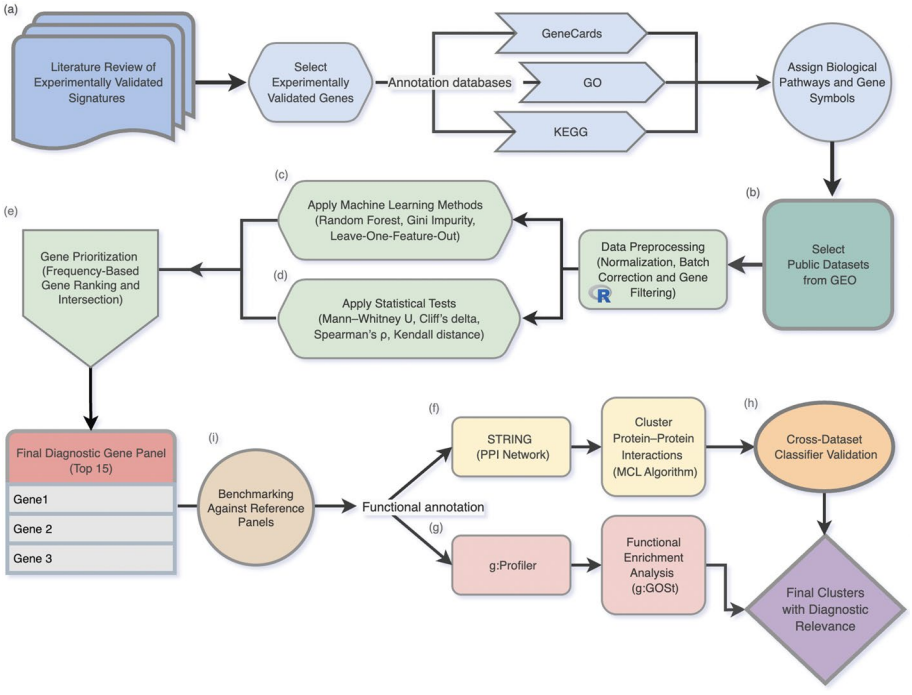

Fig. 1 Overview of the analytical pipeline used in this study. (a) Experimentally validated gene signatures were collected from literature. (b) Public transcriptomic datasets were selected from GEO. (c-d) Both machine learning models and statistical tests were applied to identify differentially expressed genes. (e) Top genes were selected based on overlap and ranking. (f-g) Functional annotation was conducted using STRING and g:Profiler g:GOSt to explore interactions and pathway enrichment. (h) Classification performance was validated, and genes were clustered based on biological relevance. (i) Benchmarking against reference panels

supported by independent experimental evidence across multiple studies or cohorts, rather than originating from a single dataset or publication. Priority was given to biomarkers validated using quantitative assays (such as RT-qPCR, ELISA, or Western blot) and/or functional perturbation studies in animal or cellular models. To maintain translational relevance, we excluded genes lacking experimental support, such as those identified solely through in silico predictions.

Each candidate gene was annotated using official gene symbols and aliases from the GeneCards database [18], ensuring consistent nomenclature and preventing redundancy due to alternative naming conventions. The resulting panel comprised 55 genes supported by experimental evidence and linked to immune dysregulation in sepsis. Although this panel includes genes participating in overlapping immune pathways, such redundancy was intentionally retained at this stage to allow data-driven prioritization and identification of the most stable and informative markers during subsequent multi-cohort statistical and machine-learning analyses.

To enhance interpretability, we grouped these selected genes into five functional categories based on annotations from GeneCards, the Kyoto Encyclopedia of Genes and Genomes (KEGG) [19], and the Gene Ontology (GO) resource [20–22].

These categories reflect major molecular components of the host response to infection and highlight key hallmarks of sepsis, including excessive inflammation, immune suppression, vascular injury, and disrupted intracellular signaling, which are summarized in Table 1. This biologically grounded gene panel served as the foundation for subsequent statistical analysis, machine learning modeling, and functional enrichment workflows [23–52].

2.2 GEO search and data preprocessing

We systematically retrieved sepsis-related transcriptomic datasets from the Gene Expression Omnibus (GEO) (step *b* in Fig. 1) [53] to ensure broad coverage and reproducibility across independent studies. Datasets were included if they met the following criteria: (First) explicit annotation of sepsis or septic shock cases and corresponding healthy or non-septic controls in their metadata; (Second) availability of raw or normalized gene expression data encompassing the 55 genes of our curated panel; and (Third) a minimum sample size of 30 to ensure adequate statistical power.

In total, 14 datasets satisfied these criteria. Of these, 11 independent cohorts were used for model training and gene prioritization, while 3 additional datasets were reserved exclusively for external validation of biological relevance and diagnostic performance.

Table 1 Curated sepsis-related gene signature categorized by biological pathways (gene symbols from GeneCards)

Pathway	Genes
Innate immune activation and inflammation	TNF, IL1B, IL6, IFNG, CXCL8, CXCL10, S100A8, S100A9, S100A12, TREM1, CCR2, CCL2, FCGR1A, TLR2, TLR4, CD14, MYD88, NLRP3, P2RX7, LBP, HMGB1, OLFM4, LCN2, IFNA1, IFNA2, IFNB1, ITGAM
Adaptive immune suppression and apoptosis	IL10, IL1R2, PDCD1, BCL2, SOCS3, HLA-DRA, TNFSF10, CCR7, CCL19, ARG1
Complement and coagulation pathways	C3AR1, C5AR1, CRP, ELANE, PTX3
Endothelial dysfunction and vascular response	ICAM1, VCAM1, CX3CR1, CALCA, PLAUR, MMP8, MMP9, CD177
Transcriptional regulation and signaling pathways	MAPK14, NOTCH1, HIF1A, LCN2, GATA3

All preprocessing and analytical steps were performed using the R programming language (version 4.4.2). The study includes both bulk RNA-seq and microarray datasets, which required platform-specific preprocessing. Raw RNA-seq datasets were normalized using the `DESeq2` package with variance stabilizing transformation (VST) [67], while microarray datasets were normalized using the `limma` package [68]. Batch effect correction was applied using the ComBat algorithm from the `sva` R package when applicable, strictly within individual datasets, to address known technical batches, and never across different cohorts or platforms [69, 70]. Importantly, analyses were kept strictly separate at the dataset and platform level, and no joint normalization or merging of RNA-seq and microarray expression matrices was performed. Datasets that were already normalized by the original authors were utilized without additional transformation. For datasets containing multiple sampling time points, we selected the earliest available sample to capture early transcriptional responses relevant to sepsis onset. If explicit time-point metadata were unavailable, all available samples were included.

A summary of the selected datasets, including their experimental platforms, sample sizes, and normalization methods used for model training is provided in Table 2a and for external validation is provided in Table 2b.

To account for heterogeneity across cohorts, each dataset was analyzed independently throughout preprocessing, modeling, and evaluation. Raw expression matrices were not merged across studies, thereby avoiding artificial cross-study batch effects and preserving dataset-specific biological and clinical context. Differences in biospecimen type (whole blood, leukocyte-enriched samples, or peripheral blood mononuclear cells), transcriptomic platform (RNA-seq or microarray), and sampling protocols are explicitly reported in Table 2a, b and may contribute to variation in effect sizes across cohorts.

Regarding clinical definitions, most publicly available GEO datasets provide only binary case labels ("sepsis" versus "control") without detailed annotation of diagnostic criteria (such as, Sepsis-2, Sepsis-3, or institution-specific definitions). We therefore

Table 2 Overview of datasets used in this study. (A) Training and gene selection cohorts. (B) External validation cohorts

(a) Datasets used for model training and gene selection			
Dataset	**Platform**	**#Samples**	**Sample type, normalization, source**
GSE185263	RNA-seq, Illumina HiSeq 2500	392	Whole blood, DESeq2 [54]
GSE65682	MA, Affymetrix U219	234	Whole blood, RMA [55]
GSE236713-D1	MA, Agilent SurePrint G3 8×60K	155	Leukocytes, 75th Pctl norm [56]
GSE131761	MA, Agilent Whole Genome 4×44K	96	Whole blood, limma [57]
GSE54514	MA, Illumina HumanHT-12 v3.0	71	Whole blood, BRB-ArrayTools [58]
GSE154918	RNA-seq, Illumina HiSeq 4000	79	Peripheral blood, DESeq2 [59]
GSE96063-T0	MA, Affymetrix Human Gene 2.1 ST	52	Peripheral blood, RMA
GSE57065_hr0	MA, Affymetrix Genome U133 Plus 2.0	53	Leukocytes, RMA [60]
GSE100159	MA, Illumina HumanWG-6 v3.0	45	Whole blood, limma [61]
GSE243217	RNA-seq, MGISEQ-2000RS	37	PBMCs, DESeq2 [62]
GSE28750	MA, Affymetrix U133 Plus 2.0	30	Whole blood, RMA [63]
(B) Datasets used for external validation			
Dataset	**Platform**	**#Samples**	**Sample type, Normalization, Source**
GSE69528	MA, Illumina HumanHT-12 v4.0	112	Whole blood, Quantile + log2 [64]
GSE60424	RNA-seq, Illumina HiScanSQ	49	Whole blood, DESeq2 [65]
GSE63311	RNA-seq, Illumina Genome Analyzer IIx	49	Whole blood, DESeq2 [66]

When multiple time points were available, only the earliest was analyzed (D1 = Day 1, T0 = emergency admission, hr0 = within 30 min of shock). PBMCs: peripheral blood mononuclear cells. RMA: robust multi-array average. MA: microarray

retained the original classifications as reported by the dataset authors and treated this variability as an inherent characteristic of real-world sepsis cohorts. While such differences may introduce clinical heterogeneity, they also enable assessment of the robustness and reproducibility of the proposed 15-gene signature across diverse clinical contexts.

All dataset accession numbers, preprocessing steps, and analysis scripts are fully documented and publicly available. To ensure reproducibility, all code used for data preprocessing, statistical analysis, machine learning, benchmarking, and visualization is openly accessible at our GitHub repository (Software code availability section).

2.3 Machine learning-driven identification of diagnostic genes

We employed supervised machine learning using Random Forest (RF) classifiers to perform binary classification (step *c* of Fig. 1), distinguishing sepsis patients from healthy or non-septic controls based on their gene expression profiles [71]. Random Forest was selected due to its proven effectiveness in sepsis-related computational studies for both classification and feature selection [72, 73]. In addition to its demonstrated performance in prior sepsis studies, Random Forest is particularly well suited for medium-sized, high-dimensional transcriptomic data, as it can model nonlinear relationships, accommodate correlated predictors, and remain robust to noise. Importantly, RF provides stable feature-importance estimates, which are essential for downstream biological interpretation and gene prioritization in this study.

Each of the 11 training datasets was analyzed independently using the curated panel of 55 genes. To obtain reliable and unbiased estimates of model performance, we conducted 100 independent iterations per dataset, each involving a randomized, stratified 80%/20% train–test split to preserve class proportions. Random Forest classifiers were built using the following hyperparameters: the number of trees (`ntree` $= 100$) and the number of variables randomly sampled as candidates at each split (`mtry` = $\lfloor\sqrt{\text{number of features}}\rfloor$). The trees were grown fully until terminal node purity, with no explicit restriction on maximum depth. These hyperparameter values correspond to widely adopted defaults for Random Forest models applied to high-dimensional biological data and provide a well-established balance between bias, variance, and computational efficiency. Exploratory analyses using larger numbers of trees (ntree = 500) and alternative `mtry` values resulted in negligible changes in diagnostic performance, with average AUROC and MCC differences below 0.01 across datasets. Given the known robustness of Random Forest models to modest hyperparameter variation, the default configuration was retained to maximize reproducibility and comparability across cohorts.

To address class imbalance during model training, we applied the Synthetic Minority Over-sampling Technique (SMOTE) [74], configured with (K = 5) nearest neighbors. For each repeated stratified 80%/20% split, we first partitioned samples into training and test sets, and applied SMOTE exclusively to the training data. The minority class was oversampled with duplication size dynamically adjusted to match class proportions, while test sets remained untouched to prevent information leakage. To assess the impact of SMOTE on classification performance, we repeated the analysis without oversampling using class-weighted Random Forest models. AUROC and MCC values changed only marginally, indicating that SMOTE primarily improved minority-class calibration rather than artificially inflating predictive performance.

Feature importance was evaluated using the Mean Decrease in Gini impurity from the Random Forest (RF) model and further validated through a Leave-One-Feature-Out ablation analysis [75]. Additionally, to assess model robustness, controlled random noise (ranging from 10 to 50%) was introduced into the gene expression data to evaluate its impact on performance, measured by the Matthews Correlation Coefficient (MCC) [76–78].

Finally, we computed the average performance across iterations using standard classification metrics: accuracy, sensitivity (True Positive Rate, TPR), specificity (True Negative Rate, TNR), precision (Positive Predictive Value, PPV), negative predictive value (NPV), F1-score, area under the ROC curve (AUROC), and MCC. These complementary metrics provided a robust and comprehensive evaluation of diagnostic performance across heterogeneous cohorts.

2.4 Statistical analysis of diagnostic gene significance

To evaluate the statistical significance and predictive relevance of genes in our curated panel, we employed complementary nonparametric and correlation-based analyzes (step *d* of Fig. 1). The Mann–Whitney U test (Wilcoxon rank-sum test) [79, 80] was applied to compare gene expression levels between sepsis and control samples across the 11 training datasets, with adjustments for multiple testing using the Benjamini–Hochberg (BH) procedure to control the false discovery rate (FDR) [81]. Statistical significance was assessed exclusively using BH-adjusted p values. Following recent recommendations by Benjamin et al. [82], we adopted a more stringent significance threshold (p value < 0.005 rather than the traditional p value < 0.05) to minimize false-positive findings and improve reproducibility. To quantify the magnitude and direction of differential expression, Cliff's delta effect size was calculated for each gene [83]. We report effect sizes alongside BH-adjusted p values to support biological interpretation, but we do not use them as independent ranking criteria; instead, we base final gene prioritization on cross-dataset reproducibility and machine-learning-based importance measures.

We assessed the consistency between the statistical significance rankings and machine learning-based feature importance scores using Spearman's (ρ) rank correlation coefficient [84] and Kendall distance (τ) [85]. Spearman's correlation evaluates monotonic relationships, while Kendall distance quantifies pairwise concordance between rankings. Additionally, we employed bootstrapping (with one thousand resamples) to estimate robust confidence intervals for Spearman's correlation, ensuring the stability and reliability of our results [86].

This multi-level framework enabled a rigorous comparison between statistical and machine learning indicators of gene relevance across heterogeneous datasets.

2.5 Integrated gene prioritization combining machine learning and statistical evidence

To identify robust and reproducible diagnostic genes, we integrated complementary evidence from statistical testing and machine learning-based feature evaluation (step *e* of Fig. 1). Specifically, we combined the results of the Mann–Whitney U test with Benjamini–Hochberg correction and Random Forest-derived feature importance scores based on the mean decrease in Gini impurity. For each of the 11 training datasets, genes were independently ranked by adjusted p values and by Random Forest importance scores. All rankings and model evaluations were performed independently within each

dataset, and no pooled or cross-dataset modeling was conducted, thereby preventing sample-size imbalances from disproportionately influencing gene prioritization.

Genes falling within the top 25% in both rankings were considered high-confidence candidates, ensuring stringent selection criteria and enhanced reproducibility. We defined this top 25% threshold as the top 14 out of 55 genes per method per dataset. Genes that appeared in the intersection of both rankings within a dataset were retained as jointly prioritized. To ensure consistency across cohorts, we then computed how many times each gene was jointly prioritized across all 11 datasets. Genes that satisfied this criterion in at least 7 datasets were selected for inclusion in the final panel. This cross-dataset recurrence threshold balances reproducibility with biological diversity and prevents overfitting to cohort-specific signals. Importantly, genes showing inconsistent behavior (such as ranking highly in only one or two datasets or demonstrating conflicting importance trends) were excluded from the final panel.

To visualize and validate the agreement between statistical and machine learning rankings, we generated Venn diagrams displaying the intersecting sets of top-ranked genes [87]. Genes consistently identified by both analytical methods were prioritized for subsequent functional enrichment and biological interpretation, forming the final diagnostic gene set used in downstream analyzes.

2.6 Benchmarking against established reference panels

To contextualize the diagnostic performance of the proposed 15-gene panel, we benchmarked it against three widely cited sepsis gene signatures: the SeptiCyte LAB panel (PLA2G7, CEACAM4, LAMP1, PLAC8) [88], the Stanford 11-gene panel [89], and the FAIM3/PLAC8 ratio [90]. These comparators collectively represent commercial, academic, and minimal-gene diagnostic strategies.

We benchmarked all comparator signatures across six independent datasets. For each dataset, we extracted expression values corresponding to the comparator gene panels and evaluated them using the same supervised learning framework applied to our proposed signature, thereby ensuring methodological consistency across models.

Specifically, We applied identical preprocessing procedures to all comparator panels, mirroring those used for our signature: DESeq2 variance-stabilizing transformation for RNA-seq data, limma normalization for microarray datasets, and ComBat correction for batch effects when necessary. We also addressed class imbalance using the same strategy as in the primary analysis, restricting any oversampling or weighting to the training partition to prevent information leakage. These precautions ensured that performance differences reflected the true diagnostic value of each gene panel rather than disparities in preprocessing, modeling, or validation.

For comparator signatures containing FAIM3/PLAC8, benchmarking was performed only in datasets where both genes were available. In datasets lacking FAIM3, models were not trained, as evaluating a two-gene signature with a single remaining gene would not constitute a meaningful or fair comparison. This constraint reflects platform-dependent gene availability rather than a limitation of the benchmarking framework.

Model performance was quantified using multiple metrics, including the Matthews Correlation Coefficient (MCC), area under the ROC curve (AUROC), F1-score, sensitivity, specificity, and precision. MCC was emphasized as the primary indicator due to its

robustness in class-imbalanced conditions and superior interpretability for binary classification tasks.

2.7 Protein–protein interaction network and cluster analysis

To investigate the functional relationships among the prioritized genes, we constructed a Protein–Protein Interaction (PPI) network using the STRING database version 12.0 (step *f* of Fig. 1) [91]. Only high-confidence interactions (combined interaction score ≥ 0.7) were included to ensure biological reliability and minimize false-positive associations, following best practices established in previous network-based studies [16].

Functional modules within the PPI network were identified using the Markov Cluster Algorithm (MCL) [92], selected for its ability to detect densely connected subgraphs based on network topology. Each resulting cluster was interpreted as a putative co-functional gene module reflecting a specific aspect of the sepsis response.

To assess the diagnostic relevance and generalizability of these clusters, we evaluated each module using the three external validation datasets listed in Table 2b. Random Forest classifiers were trained independently for each cluster to test whether its constituent genes could discriminate sepsis from controls, thereby confirming their predictive and biological robustness across independent cohorts.

2.8 Functional enrichment and pathway specificity scoring

To elucidate the biological processes and pathways significantly associated with our selected diagnostic gene set [93], we performed functional enrichment analysis using g:GOSt, part of the g:Profiler suite version e112_eg59_p19_25aa4782 (step *g* of Fig. 1) [94]. Enrichment was evaluated across Gene Ontology (GO) biological processes, KEGG pathways, and Reactome terms. Significantly enriched pathways were defined as those with an adjusted p value < 0.005.

Following statistical enrichment, pathway terms were subjected to a structured, literature-guided relevance assessment to support biological interpretation. For each pathway, we performed manual review based on published experimental and clinical studies documenting its involvement in sepsis immunopathology. We then assigned relevance scores using predefined criteria: +1 for direct implication in sepsis mechanisms, +0.5 for general molecular relevance, and -1 for pathways lacking a clear disease association. We applied this scoring framework consistently across enrichment results for both the initial 55-gene panel and the refined 15-gene signature. Importantly, these scores supported interpretive comparison only and were not used for feature selection.

3 Results

3.1 Literature-based diagnostic gene panel

A 55-gene diagnostic panel was curated through an extensive review of the biomedical literature, prioritizing genes that were experimentally validated and consistently associated with sepsis across independent studies. For biological interpretability, each gene was annotated using GeneCards, KEGG, and Gene Ontology (GO) resources, and subsequently assigned to one or more of five major functional categories (Table 1).

Several genes exhibited pleiotropic functions and were therefore classified into multiple categories. For example, IL10 contributes to both cytokine regulation and immune suppression, while MAPK14 participates in transcriptional control and stress-response

signaling. The largest functional group, Innate Immune Activation and Inflammation, encompassed a wide range of molecular types: pro-inflammatory cytokines (TNF, IL1B, IL6), chemokines (CXCL8, CXCL10), calgranulins (S100A8, S100A9, S100A12), pattern-recognition receptors (TLR2, TLR4, MYD88, CD14, HMGB1), and neutrophil-associated effectors (OLFM4, LCN2, ITGAM).

The curated panel integrates genes spanning innate immune activation, inflammation, and immunoregulation, reflecting the multifaceted nature of sepsis pathophysiology.

3.2 Machine learning-based gene prioritization

Random forest (RF) classifiers achieved consistently strong performance across the 11 independent sepsis datasets, confirming the robustness of gene expression-based classification for early sepsis detection. Average performance metrics were high for all indicators, with mean Matthews Correlation Coefficient (MCC) = 0.94, F1-score = 0.97, and AUROC = 0.99 (Table 3). These results demonstrate reliable discrimination between sepsis and control samples across diverse experimental platforms and cohorts.

We conducted explicit negative control analyses to rule out overfitting, including random permutation of class labels and controlled perturbation of feature noise. In both cases, classification performance declined rapidly and systematically, confirming that model accuracy relied on true biological signal rather than spurious associations.

By applying the Random Forest model independently to each dataset, we directly assessed classification stability across cohorts. Diagnostic performance remained high in most datasets (AUROC and MCC > 0.90), demonstrating robust discrimination despite transcriptomic heterogeneity. Only one dataset (GSE54514) showed a relative performance decline, with MCC dropping to approximately 0.64, although AUROC remained high at around 0.88.

The lower MCC observed in GSE54514 likely reflects cohort-specific biological and technical characteristics rather than a general limitation of the classification framework. In this dataset, feature-importance analysis revealed a partially different composition of top-ranking genes, with increased contribution from transcripts such as CD14, MYD88, and HIF1A, which were not consistently among the top features in most other cohorts. This indicates that, while sepsis-related signal remains detectable, the relative weighting of immune pathways distinguishing sepsis from controls varies across studies. Such variability may arise from differences in transcriptomic platform, preprocessing pipelines (including the use of BRB-ArrayTools), infection sources, or underlying patient immune states, all of which can influence gene-expression distributions and feature rankings in whole-blood datasets. These cohort-specific effects primarily impact class-balance-sensitive metrics such as MCC, whereas overall discrimination, as measured by AUROC, remains high. Importantly, an MCC value of approximately 0.64 still represents a substantial positive association between predicted and true class labels within the bounded

Table 3 Average performance metrics of Random Forest classification across 11 sepsis datasets

	MCC	F1-score	AUROC	TPR	TNR	PPV	NPV
Mean	0.938	0.971	0.987	0.965	0.970	0.982	0.959
SD	0.068	0.034	0.011	0.052	0.036	0.018	0.056

Values are reported as mean ± standard deviation for Matthews correlation coefficient (MCC), F1-score, area under the receiver operating characteristic curve (AUROC), true positive rate (TPR), true negative rate (TNR), positive predictive value (PPV), and negative predictive value (NPV). All metrics range from 0 to 1, except MCC (−1 to +1)

interval $[-1, +1]$, indicating meaningful diagnostic performance rather than model failure.

Feature importance analysis based on the mean decrease in Gini impurity identified a consistent subset of highly informative genes. Across datasets, the top ten features–CD177, S100A12, S100A8, GATA3, ARG1, MAPK14, S100A9, IL10, MMP9, and SOCS3–emerged as the most predictive, representing key regulators of immune activation, inflammation, and cellular stress responses.

To further evaluate the stability of gene prioritization, we performed an independent Leave-One-Feature-Out (LOFO) ablation analysis, quantifying the change in classification performance after the removal of each gene. Several of the top fifteen LOFO-ranked genes overlapped with the Gini-based consensus, while others such as TNFSF10, HIF1A, CX3CR1, and TLR2/4 were uniquely highlighted by LOFO as context-dependent contributors to model accuracy. Notably, these genes ranked between positions 15 and 30 in Gini or Mann–Whitney orderings, suggesting that they exert combinatorial effects rather than strong individual influence.

This comparison underscores the complementary nature of the two selection strategies: Gini importance favors genes that independently reduce classification error across decision trees, whereas LOFO identifies genes essential for maintaining predictive accuracy in the presence of others. Together, these analyses reveal both dominant and cooperative features within the diagnostic landscape, reinforcing the value of combining multiple selection approaches for robust biomarker discovery.

When discrepancies were observed between Mean Decrease in Gini importance and LOFO rankings, final prioritization favored genes demonstrating consistent, cross-dataset reproducibility in Gini importance combined with statistical evidence from differential expression testing. This decision reflects the fact that Gini importance, when averaged across hundreds of trees and repeated stratified iterations, provides a global and stable measure of feature relevance, whereas LOFO performance drops can be more sensitive to dataset size, local correlations among predictors, or context-specific interactions. LOFO was therefore retained as a complementary validation layer rather than a decisive selection criterion. Genes ranked highly by both Gini and LOFO were considered the most robust contributors, while genes showing divergent or unstable LOFO effects across cohorts were interpreted as potentially context-dependent and excluded from the final 15-gene panel.

3.3 Statistical validation of differential gene expression

The Mann–Whitney U test identified several genes as significantly differentially expressed between sepsis and control groups (adjusted p value < 0.005). Consistently significant genes across datasets included CD177, S100A12, S100A8, GATA3, ARG1, MAPK14, S100A9, SOCS3, IL1R2, and MMP8, many of which also ranked among the top features in the Random Forest analyses, reinforcing their diagnostic relevance (Fig. 2).

Most of these genes, such as CD177, S100A8, S100A9, and S100A12 were markedly upregulated in sepsis samples, whereas GATA3 and BCL2 were consistently downregulated across multiple datasets. The magnitude and direction of these expression changes were quantified using Cliff's delta effect sizes, confirming strong discriminatory potential for these key genes. Correlation analyses comparing statistical and machine

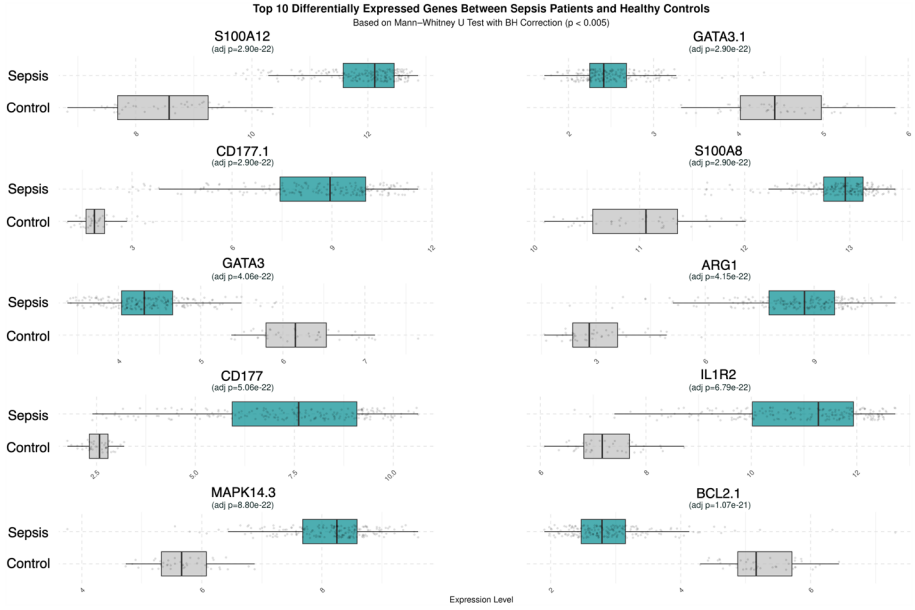

Fig. 2 Boxplots of top-ranked genes from the Mann–Whitney *U* test in dataset GSE65682 [55]. Genes shown were significantly differentially expressed between sepsis patients and healthy controls (adjusted p value < 0.005). CD177, S100A12, S100A8, and IL1R2 were upregulated; GATA3 and BCL2 were downregulated, reflecting distinct immune-dysregulation. Suffixes like ".1" or ".2" denote different microarray probes for the same gene

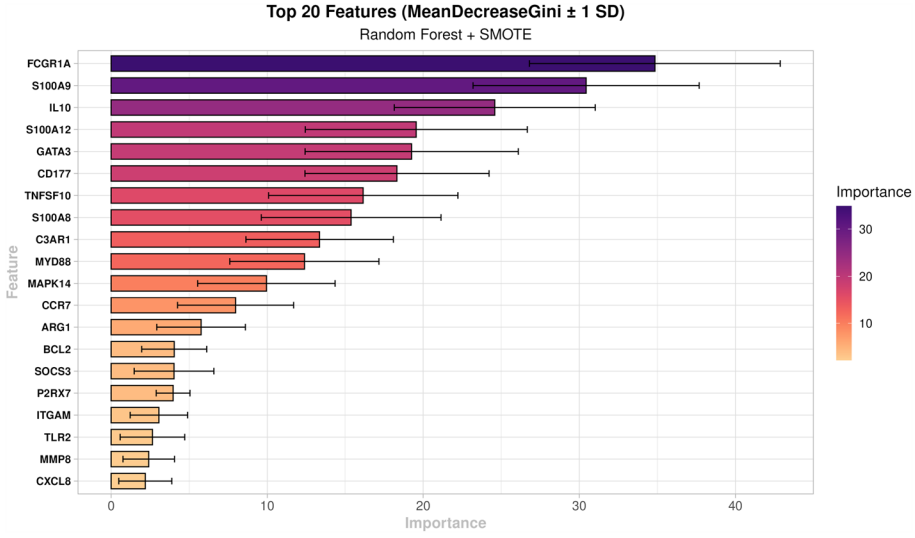

Fig. 3 Top 20 gene importances derived from Random Forest classification on dataset GSE185263 (SMOTE-balanced) [54]. Importance reflects the mean decrease in Gini index across 100 stratified resamples; error bars denote ± 1 standard deviation. Genes are colored by average importance (viridis scale). This ensemble evaluation enhances robustness and mitigates sampling bias

learning-based rankings demonstrated strong agreement, with mean Spearman's rank correlation ($\rho = 0.91$) and Kendall's tau distance ($\tau = 0.76$) across all 11 datasets. Bootstrapping with one thousand resamples confirmed the robustness of these correlations and the stability of gene prioritization across heterogeneous cohorts (Figs. 3, 4).

Figure 5 illustrates the strong concordance between Mann–Whitney-based and Random Forest-based gene rankings, while Fig. 4 visualizes the expression patterns in dataset GSE185263 [54]. Genes positioned toward the upper extremes of the volcano

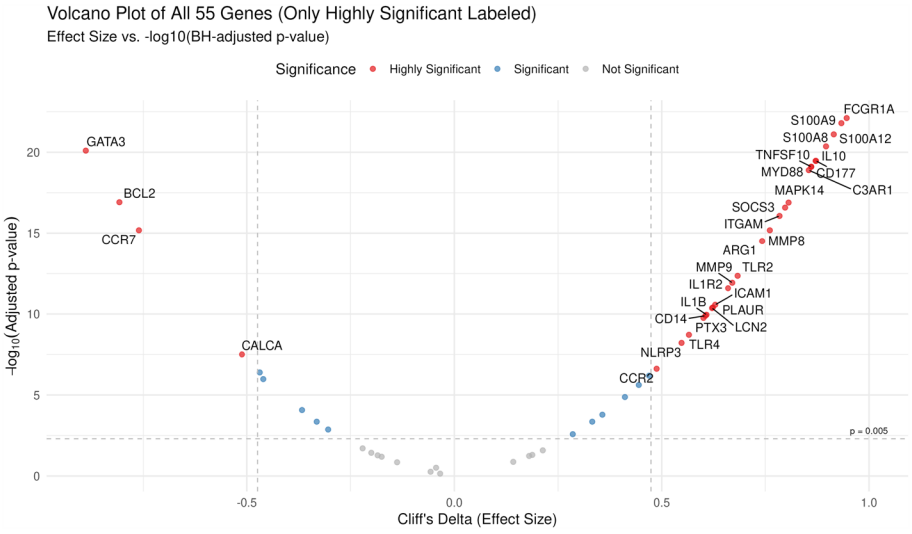

Fig. 4 Volcano plot of gene expression in dataset GSE185263 [54]. The *x*-axis shows Cliff's delta; the *y*-axis shows $-\log_{10}$ of BH-adjusted *p* values from Mann–Whitney *U* tests. Dashed lines indicate thresholds for effect size ($|\delta| \geq 0.4$) and significance ($p < 0.005$). Red dots are highly significant genes, blue are significant with lower effect sizes, and gray are non-significant. Genes on the right are upregulated; those on the left are downregulated

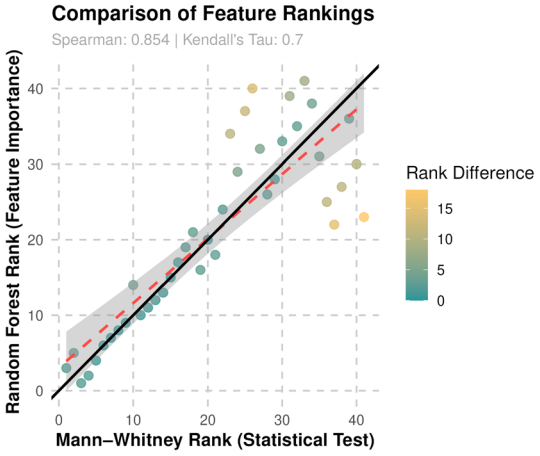

Fig. 5 Scatter plot comparing gene rankings from the Mann–Whitney *U* test (*x*-axis) and Random Forest Gini importance (*y*-axis) for dataset GSE65682 [55]. Each dot represents a gene, colored by absolute rank difference. The black line indicates perfect agreement; the red dashed line shows the regression fit with a 95% confidence interval. Spearman's $\rho = 0.854$ and Kendall's $\tau = 0.7$ indicate strong concordance between methods

plot (combining large effect sizes and high statistical significance) represent the most robust diagnostic biomarkers of sepsis.

3.4 Consensus selection of core diagnostic genes

To identify the most robust diagnostic biomarkers, we integrated gene rankings obtained from both the Random Forest feature importance analysis and the Mann–Whitney U test across all 11 datasets. Genes that consistently appeared within the top quartile of both ranking methods were considered highly reliable candidates. This consensus strategy yielded a reproducible 15-gene panel comprising S100A12, S100A9, S100A8, ITGAM, CD177, FCGR1A, C3AR1, IL10, IL1R2, GATA3, SOCS3, MAPK14, MMP9, BCL2, and ARG1. Their recurrent prominence across independent datasets and

complementary analytical approaches indicates a shared biological signature strongly associated with immune modulation and inflammatory signaling in sepsis.

Subsequent analyses explore the functional relationships among these genes through Protein–Protein Interaction (PPI) network analysis, providing a systems-level view of their coordinated roles in sepsis pathophysiology.

3.5 Diagnostic performance benchmarking

Across six independent datasets, the proposed 15-gene panel consistently outperformed all reference signatures, achieving higher Matthews correlation coefficient (MCC) and AUROC values (Fig. 6).

The FDA-approved SeptiCyte LAB assay demonstrated high AUROC values (0.819–0.992) but inconsistent MCC across datasets, ranging from 0.392 (GSE63311) to 0.901 (GSE236713). In contrast, the 15-gene panel maintained uniformly strong performance, with MCC consistently above 0.83 in all cohorts, including those with higher class imbalance. This stability indicates improved generalization and resilience to data heterogeneity.

The academic 11-gene signature achieved reasonably well performance but includes several genes (ZDHHC19, RPGRIP1, KIAA1370) with limited mechanistic relevance to sepsis. Previous studies have shown that exclusion of these genes minimally affects performance, raising concerns about the biological coherence of the panel. By contrast, all genes in our 15-gene panel were selected through an integrative framework combining Random Forest feature importance, Mann–Whitney U tests, correlation analysis, and functional enrichment, ensuring both diagnostic strength and biological interpretability.

The minimal 2-gene FAIM3/PLAC8 signature within the three datasets where both FAIM3 and PLAC8 were present achieved strong diagnostic performance, with Matthews Correlation Coefficient (MCC) values ranging approximately from 0.77 to 0.95, consistent with previously reported results in the literature. Beyond diagnostic performance, minimal signatures such as FAIM3/PLAC8, do not provide sufficient dimensionality to support characterization of immune-response. The multi-gene composition of the proposed 15-gene panel enables simultaneous assessment of coordinated innate,

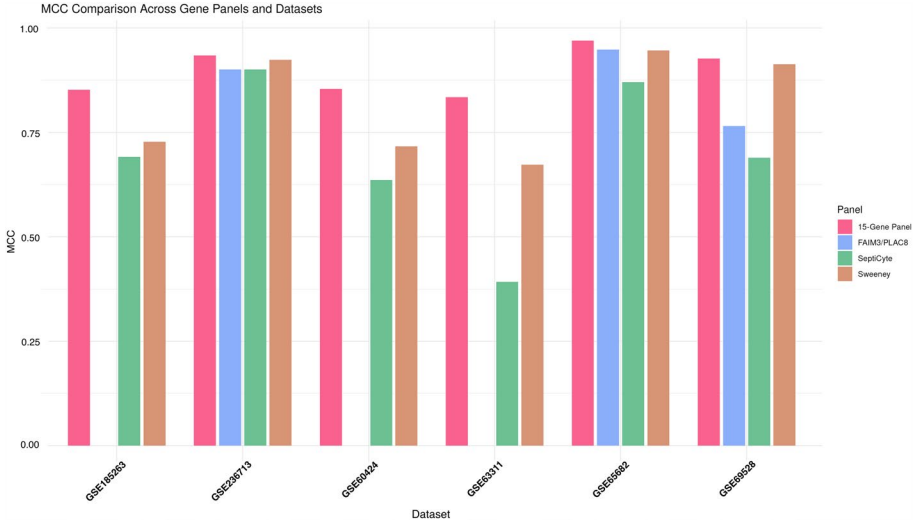

Fig. 6 Benchmarking of diagnostic accuracy (MCC) for the 15-gene panel compared to three reference signatures across six datasets

regulatory, and suppressive transcriptional programs, allowing diagnostic classification to be accompanied by module-level biological stratification.

Because the native scoring algorithms or decision rules of some reference signatures (such as, SeptiCyte LAB and ratio-based panels) are proprietary, fixed, or not directly transferable to public transcriptomic datasets, their original clinical implementations cannot be faithfully reproduced. Accordingly, all comparator gene sets were evaluated using the same Random Forest framework applied to the proposed panel, enabling a standardized comparison of gene-set-level diagnostic information rather than replication of their native assays.

Figure 6 summarizes performance differences across the evaluated panels. While AUROC values were generally high for all models, MCC provided a more discriminative and clinically meaningful metric. For instance, in dataset GSE63311, both our panel and SeptiCyte LAB achieved high AUROC (0.987 vs. 0.819), yet MCC diverged markedly (0.834 versus 0.392), reflecting superior balance between sensitivity and specificity. Across all datasets, the 15-gene panel achieved the highest mean MCC and AUROC values, underscoring its robustness, reproducibility, and clinical applicability for sepsis diagnosis.

3.6 Protein–protein interaction network and cluster analysis

To investigate functional interactions among the prioritized diagnostic genes, we constructed a high-confidence Protein–Protein Interaction (PPI) network using the STRING database, applying a stringent interaction score threshold (score ≥ 0.7) to ensure biologically relevant and experimentally supported connections. Application of the Markov Cluster Algorithm (MCL) revealed three distinct gene clusters, each representing a key component of the sepsis host immune response (Figs. 7, 8).

Cluster 1 (Red)—Immune regulation and apoptosis. Cluster 1 comprises IL10, BCL2, SOCS3, GATA3, MAPK14, ARG1, IL1R2, and MMP9. This cluster features genes involved in anti-inflammatory signaling, immune cell apoptosis, and the compensatory anti-inflammatory response (CARS) in sepsis. Several of these genes, IL10, IL1R2, SOCS3, and ARG1 are key regulators of the immunosuppressive response and have been independently associated with adverse clinical outcomes in sepsis. IL10 is a hallmark anti-inflammatory cytokine that inhibits T-cell activation and promotes regulatory immune phenotypes; elevated IL10 levels correlate with increased severity and mortality [95]. IL1R2 encodes a decoy receptor for IL-1β, which sequesters pro-inflammatory signals without transducing them, and its expression rises rapidly in sepsis [96, 97]. SOCS3, induced by IL10 and other cytokines, inhibits JAK/STAT signaling and contributes to the phenomenon of endotoxin tolerance in monocytes and macrophages [98, 99]. ARG1, typically produced by neutrophils and myeloid-derived suppressor cells, depletes arginine, a key nutrient for T-cell function, thus impairing adaptive immune responses and exacerbating sepsis-induced immune dysfunction [100, 101]. MMP9 and MAPK14 (p38 MAPK) promote tissue remodeling and inflammation resolution, indicating attempts to recover from early tissue damage [32, 102]. Conversely, BCL2 and GATA3 are downregulated, indicating reduced lymphocyte survival and impaired Th2-mediated responses. GATA3 is a master regulator of Th2 differentiation, and its suppression in sepsis reflects a shift away from adaptive immunity [103]. BCL2, an anti-apoptotic gene essential for lymphocyte survival, is often reduced in septic patients and has been linked

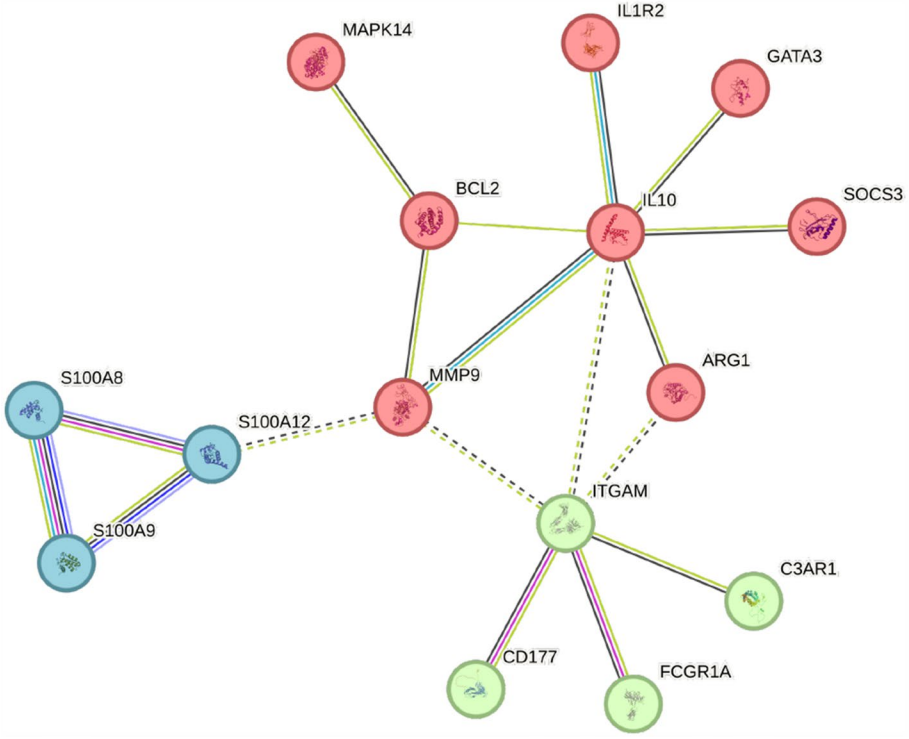

Fig. 7 Protein–protein interaction (PPI) network of 15 diagnostic genes generated using STRING (confidence score ≥ 0.7). The network reveals biologically meaningful interactions forming distinct gene clusters

color	cluster Id	gene count	description
	cluster 1	8	1. Negative regulation of epithelial cell apoptotic process 2. CD163 mediating an anti-inflammatory response
	cluster 2	4	Positive regulation of myeloid leukocyte mediated immunitv
	cluster 3	3	1. RAGE receptor binding 2. Metal sequestration by antimicrobial proteins, and Regulation of endothelin production

Fig. 8 Summary of functional annotations for the three gene clusters identified in the PPI network using the Markov Cluster Algorithm (MCL). Each cluster represents distinct immune-related processes relevant to sepsis pathophysiology

to lymphopenia and immunoparalysis [104]. The reproducibility of these patterns across datasets reflects the transition from hyperinflammation to immune exhaustion, highlighting potential therapeutic targets for restoring immune balance.

Cluster2 (Green)—Myeloid cell activation and complement signaling. This cluster includes ITGAM, CD177, C3AR1, and FCGR1A, all significantly upregulated in sepsis and indicative of a neutrophil-driven innate immune response. These genes encode

surface receptors and effectors characteristic of activated neutrophils and monocytes, aligning with clinical evidence that neutrophil activation is a hallmark of sepsis. ITGAM (integrin αM, CD11b) and FCGR1A (FcγRI, CD64) are strongly induced on phagocytes, promoting leukocyte adhesion and phagocytosis; notably, FCGR1A is already used as a diagnostic marker in critically ill patients [105]. C3AR1, encoding the receptor for complement fragment C3a, links complement activation to downstream inflammatory cascades. CD177, a neutrophil-specific surface protein, is elevated in sepsis, correlates with severity, and marks a hyperactive subset capable of endothelial transmigration and granule release, contributing to both antimicrobial defense and tissue damage. These findings underscore the dual role of neutrophils in sepsis, as they are indispensable for pathogen clearance but can cause significant tissue damage when overactivated [106, 107]. Consistent with these mechanisms, Cluster 2 demonstrated strong diagnostic performance and may represent a biomarker of innate immune dysregulation as well as a potential target for neutrophil-directed immunomodulatory therapies.

Cluster 3 (Blue)—Calgranulin-mediated innate defense. This cluster consists of S100A8, S100A9, and S100A12, members of the calgranulin family and among the most highly upregulated transcripts in sepsis. These genes encode damage-associated molecular pattern (DAMP) proteins that amplify innate immune responses. S100A8 and S100A9 form the heterodimer calprotectin, while S100A12 (EN-RAGE) is a closely related protein. All three are abundantly released by activated neutrophils and monocytes during acute inflammation. Functioning as endogenous danger signals, calgranulins bind to pattern recognition receptors such as Toll-like receptor 4 (TLR4) and the receptor for advanced glycation end products (RAGE), propagating inflammatory signaling [108]. Mechanistically, they promote cytokine release, leukocyte recruitment, endothelial adhesion molecule expression, and metal ion sequestration such as zinc, to inhibit microbial growth. Their overexpression contributes to systemic inflammation, capillary leak, and coagulopathy, hallmark features of severe sepsis. Elevated plasma levels of S100A8/A9 correlate with sepsis severity, and calprotectin is already being explored as a promising clinical biomarker [109]. These findings support the diagnostic and therapeutic potential of targeting S100-RAGE/TLR4 signaling to mitigate inflammation and vascular injury in sepsis [110].

3.7 Cluster-level validation of diagnostic performance

To assess the diagnostic contribution of each gene cluster (step *h* of Fig. 1), we trained independent Random Forest classifiers using only the genes within each cluster and evaluated their performance across three external validation datasets (GSE69528, GSE60424, and GSE63311) [64–66]. Performance metrics were summarized as mean Matthews Correlation Coefficient (MCC), Area Under the ROC Curve (AUROC), and other standard classification indicators across these datasets.

Cluster 3, composed primarily of calgranulin family genes that mediate neutrophil-driven inflammation, achieved the strongest predictive performance (MCC = 0.849, AUROC = 0.967), followed by Cluster 1 (MCC = 0.804, AUROC = 0.969) and Cluster 2 (MCC = 0.723, AUROC = 0.944). These findings highlight the diagnostic prominence of neutrophil-associated danger signaling (Cluster 3) in early sepsis detection. Despite the performance differences, all clusters maintained robust classification metrics, underscoring the multifactorial nature of sepsis pathophysiology. Notably, while the

calgranulin-dominated Cluster 3 encompassing the calprotectin subunit genes S100A8 and S100A9, captures a strong hyperinflammatory signal comparable to single-marker calprotectin baselines, the full 15-gene panel integrates additional immune programs that extend diagnostic robustness and biological interpretability beyond neutrophil activation alone. Together, these results suggest that accurate sepsis diagnostics likely require the integration of signals from multiple biological processes, including inflammation, immune suppression, and endothelial dysfunction, rather than reliance on a single molecular mechanism.

To provide a quantitative comparison, Table 4 summarizes the average diagnostic metrics for each cluster and for the full 15-gene panel. While Cluster 3 performed best individually, the full gene panel achieved slightly higher overall accuracy and robustness, indicating synergistic effects among the three functional modules. This supports the concept that the 15-gene signature integrates complementary biological signals for improved diagnostic generalizability.

Taken together, the external validation confirms the robustness and interpretability of the modular 15-gene diagnostic signature, demonstrating that its constituent clusters contribute distinct yet complementary biological information relevant to sepsis pathophysiology.

To further validate the biological relevance of Cluster 3 (calgranulin genes: S100A8, S100A9, and S100A12), we performed single-cell gene expression analysis on peripheral blood mononuclear cell (PBMC) data obtained from the Single Cell Portal database (study SCP548) [111]. This analysis revealed high expression of these genes predominantly in monocytes and megakaryocytes. While neutrophils (the primary source of calgranulins during acute inflammation) are absent from PBMC datasets, their expression in monocytes aligns with known roles of these cells in amplifying systemic inflammation in sepsis [112]. Moreover, emerging evidence suggests that megakaryocytes actively contribute to inflammatory signaling in sepsis, further underscoring the diagnostic and mechanistic significance of Cluster 3 [113].

To validate the cellular origin and biological specificity of the diagnostic modules, we analyzed the publicly available single-cell RNA-seq dataset SCP548 from the Single Cell Portal [111]. This dataset profiles 126,351 peripheral blood mononuclear cells (PBMCs) from 29 sepsis patients and 36 healthy controls using the 10x Genomics 3' v2 platform, annotated into canonical immune subsets including monocytes, megakaryocytes, dendritic cells, NK cells, T cells, and B cells. Because mature neutrophils are underrepresented in PBMC preparations, single-cell validation primarily focused on genes expressed in monocyte-accessible modules–most notably Cluster 3 (calgranulin module).

Within SCP548, the calgranulin genes S100A8, S100A9, and S100A12 showed strong upregulation in septic patients compared with controls, with expression concentrated

Table 4 Average diagnostic performance of each gene cluster and the full 15-gene panel across three validation datasets

Cluster	MCC	F1-score	AUROC	TPR	TNR	PPV	NPV
Cluster 1	0.804	0.900	0.969	0.877	0.921	0.952	0.869
Cluster 2	0.723	0.886	0.944	0.853	0.874	0.946	0.871
Cluster 3	0.849	0.943	0.967	0.924	0.935	0.971	0.871
Full 15-gene panel	0.871	0.942	0.987	0.918	0.961	0.981	0.865

in monocytes and, to a lesser extent, in megakaryocytes. Although neutrophils, the primary source of calgranulins during acute inflammation are absent from PBMC datasets, their strong expression in monocytes aligns with the established pro-inflammatory role of these cells in sepsis [112]. Furthermore, recent evidence implicates megakaryocytes as active participants in systemic inflammation, contributing cytokines and chemokines that amplify immune responses [113]. This pattern confirms the calgranulin module as a dominant inflammatory signature in circulating immune cells and supports its detectability in routine blood samples.

Other modules were less represented in PBMCs. Cluster 2 genes (ITGAM, FCGR1A, C3AR1, CD177) showed moderate monocyte and megakaryocyte expression, consistent with their myeloid and complement functions, whereas CD177 was nearly absent due to its neutrophil specificity. The absence of CD177 in PBMC-based single-cell datasets reflects the exclusion of mature neutrophils during PBMC isolation rather than a lack of biological relevance. Accordingly, CD177 validation is more appropriately performed in whole-blood or leukocyte-retaining transcriptomic and cytometric assays. Cluster 1 genes exhibited weak or sparse PBMC expression, indicating activation in cell types not captured in this dataset.

Overall, single-cell analysis confirms that the diagnostic modules are transcriptionally active in circulating immune cells, with Cluster 3 emerging as the most robust and cell-type-specific component of the 15-gene signature.

3.8 Functional enrichment and pathway scoring results

To assess the biological coherence of the refined 15-gene panel compared with the original 55-gene pool, we performed functional enrichment analysis using the g:GOSt module of the g:Profiler suite (adjusted p value < 0.005). Each enriched pathway was assigned a sepsis relevance score based on literature evidence: +1 for sepsis-specific processes, +0.5 for generally immune-related functions, and -1 for nonspecific or unrelated pathways.

The initial 55-gene panel was enriched for 19 biological processes, including core immune functions such as cytokine signaling, lipopolysaccharide (LPS) binding, and leukocyte adhesion, but also nonspecific terms like collagen metabolism and sensory perception. This broad enrichment profile yielded a cumulative relevance score of 9.5 (average 0.50 per pathway), reflecting partial but diluted sepsis specificity (Fig. 9).

In contrast, the refined 15-gene subset revealed a more compact enrichment profile, with 14 pathways tightly focused on mechanisms central to sepsis immunopathology, including Toll-like receptor 4 (TLR4) signaling, RAGE receptor binding, neutrophil aggregation, and apoptotic regulation. Despite fewer total pathways, the subset retained the same cumulative relevance score (9.5) and raised the mean pathway specificity to 0.68, indicating greater biological precision.

Importantly, this reduction in the number of enriched pathways reflects the elimination of peripheral or weakly disease-associated processes present in the broader panel, rather than a narrowing of biological scope. The refined 15-gene panel concentrates enrichment within pathways that are consistently implicated in pathogen sensing, innate immune amplification, and immune regulation, core hallmarks of sepsis pathophysiology (Fig. 10). Together, these results demonstrate that systematic integration of statistical testing, machine learning prioritization, and literature-guided biological

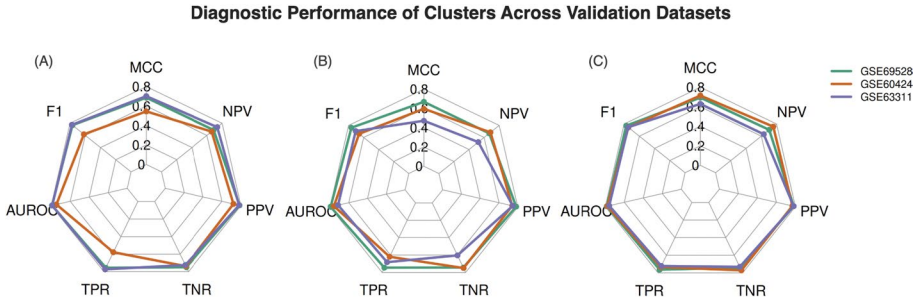

Fig. 9 External validation of cluster-specific Random Forest classifiers across three datasets (GSE69528, GSE60424, and GSE63311). Radar plots illustrate diagnostic performance for **A** Cluster 1, **B** Cluster 2, and **C** Cluster 3, measured by Matthews Correlation Coefficient (MCC), F1-score, AUROC, True Positive Rate (TPR), True Negative Rate (TNR), Positive Predictive Value (PPV), and Negative Predictive Value (NPV). Cluster 3 displayed the highest overall and most consistent performance across validation datasets

ID	Term Name For 55 Genes	Padj	Relevance Score	Term Name For Top 15 Genes	Padj	Relevance Score
1	Signaling receptor binding	9.900x10^-23	0.5	RAGE receptor binding	1.027x10^-5	1
2	Lipopolysaccharide binding	4.677x10^-7	1	Calcium-dependent protein binding	7.808x10^-5	0.5
3	Immune receptor activity	2.179x10^-6	1	Toll-like receptor 4 binding	7.997x10^-4	1
4	Cytokine binding	5.048x10^-6	1	Arachidonate binding	2.795x10^-3	0.5
5	Lipopolysaccharide immune receptor activity	1.711x10^-4	1	Defense response	1.365x10^-5	1
6	Inflammatory response	4.259x10^-45	1	Cell-cell adhesion	3.941x10^-6	1
7	Leukocyte cell-cell adhesion	1.199x10^-25	1	Positive regulation of molecular function	4.361x10^-6	0.5
8	Positive regulation of calcidiol 1-monooxygenase activity	2.418x10^-5	-1	Regulation of metabolic process	1.083x 10^-4	0.5
9	Positive regulation of DNA binding	8.210x10^-5	0.5	Regulation of intrinsic apoptotic signaling pathway	#cce31c	1
10	Membrane protein ectodomain proteolysis	3.140x10^-6	0.5	Sequestering of zinc ion	6.425x10^-4	-1
11	Collagen metabolic process	3.750x 10^-4	-1	Neutrophil aggregation	8.476x10^-4	1
12	Positive regulation of transcription by RNA polymerase II	3.184x10^-6	0.5	Leukocyte differentiation	2.813x10^-7	1
13	Endothelium development	2.412x10^-3	1	Secretory granule	1.417x10^-7	0.5
14	Sensory perception of pain	4.350x10^-3	-1	Calprotectin complex	5.505x10^-5	1
15	Antimicrobial humoral immune response mediated by antimicrobial peptide	1.846x10^-7	1	_	_	9.5
16	Extracellular region	1.101x10^-15	0.5			
17	Secretory granule	1.190x10^-14	0.5			
18	Cell surface	1.190x10^-14	0.5			
19	Calprotectin complex	1.400x10^-3	1			
_	_	_	9.5			

Fig. 10 Comparison of g:Profiler g:GOSt enrichment results for the 55-gene panel and the refined 15-gene subset (adjusted $p < 0.005$). Columns include term name, adjusted p value, and relevance score (1 = highly relevant to sepsis, 0.5 = moderate, -1 = unrelated). Only significant terms are shown

filtering improves not only diagnostic performance but also mechanistic coherence and interpretability.

4 Discussion

This study identified a reproducible 15-gene transcriptional signature that robustly distinguished sepsis from non-septic controls across 11 independent cohorts. The panel exhibited strong diagnostic performance and cross-cohort stability. Of the 15 genes, thirteen were consistently upregulated, reflecting activation of innate immune pathways, while two genes (GATA3 and BCL2) were downregulated, consistent with lymphocyte apoptosis and immunosuppressive signaling [42, 52]. Collectively, this expression pattern recapitulates the hallmark biphasic immune dysregulation of sepsis, characterized by hyperinflammatory and immunosuppressive responses.

When benchmarked against three widely cited reference panels, the proposed 15-gene signature demonstrated superior diagnostic performance and enhanced biological

interpretability. Unlike previous signatures that often include genes with unclear mechanistic ties to sepsis, the current panel was derived using an integrative framework that combined differential expression analysis, Random Forest-based feature selection, and pathway-informed refinement. While each method is well established, the novelty of this approach lies in its comprehensive integration across 11 independent cohorts, systematic benchmarking against clinically validated assays, and prioritization of mechanistically relevant genes. Consequently, all genes in the final panel map to well-characterized components of the sepsis immune response, providing both diagnostic utility and biological insight.

Network clustering and pathway enrichment further stratified the 15 genes into three functionally distinct modules that capture complementary axes of the sepsis immune response. Cluster 1 represents the immunosuppressive arm of sepsis, integrating adaptive immune regulation, apoptotic signaling, and anti-inflammatory feedback. This module is consistent with the compensatory anti-inflammatory response syndrome (CARS) [114], a clinically recognized phase in which the immune system shifts from early hyperactivation toward systemic hypo-responsiveness. Elevated expression of key mediators such as IL10, IL1R2, SOCS3, and ARG1, combined with reduced expression of lymphocyte survival genes like BCL2 and Th2-associated regulators such as GATA3, defines a transcriptional signature associated with impaired pathogen clearance and heightened vulnerability to secondary infections [95, 115]. These genes, particularly IL10, IL1R2, and ARG1, have been recurrently identified in transcriptomic studies as markers of poor prognosis and have been linked to sepsis endotypes characterized by lymphocyte exhaustion and monocyte dysfunction [116–119]. Accordingly, Cluster 1 captures a robust immunoparalysis module and may support endotype-specific stratification, identifying patients who are unlikely to benefit from further immunosuppression and may instead require immune-restorative therapies.

Cluster 2 reflects a canonical innate immune activation module dominated by neutrophil- and monocyte-associated genes. Multiple transcriptomic and functional studies have implicated this cluster in the pathophysiology of sepsis [120]. CD177, for instance, is one of the most upregulated transcripts in septic neutrophils and is associated with enhanced degranulation and transendothelial migration [121]. Clinically, dynamic increases in the CD177/CD10 ratio, indicating a shift toward immature, activated neutrophils have been shown to predict 7-day mortality in critically ill patients [122]. FCGR1A (CD64), a well-established sepsis biomarker, is routinely used to differentiate bacterial sepsis from non-infectious SIRS. Higher FCGR1A expression has also been associated with improved survival in sepsis, potentially reflecting a preserved or competent innate response [39]. ITGAM (CD11b), a key integrin mediating leukocyte adhesion and pathogen recognition, contributes to sepsis-induced inflammation through HMGB1 signaling; its blockade has been shown to improve survival in experimental models [27]. C3AR1, another key gene in this module, has emerged as a hub in sepsis gene networks, with its expression promoting MAPK pathway activation and inflammatory macrophage polarization [27, 123]. Taken together, Cluster 2 represents a neutrophil-dominant hyperinflammatory endotype, frequently observed in transcriptomic sepsis subtypes associated with poor outcomes. Its strong link to innate immune activation supports its potential utility as a biomarker of early hyperinflammation and disease severity.

Cluster 3 captures a damage-associated molecular pattern (DAMP)-driven inflammatory module centered on the calgranulin family. These genes are well established as early amplifiers of inflammation in sepsis. Transcriptomic and proteomic studies consistently show marked upregulation of calgranulins in severe sepsis and septic shock. For instance, single-cell RNA-seq of peripheral blood mononuclear cells from septic patients revealed sustained expression of an S100A8/A9 signature in monocytes from the preclinical to overt sepsis phase, particularly in high-risk patients [124]. Proteomic profiling similarly demonstrates significantly elevated plasma levels of S100A8/A9 (calprotectin) and S100A12 in septic shock patients compared to healthy controls ($P < 0.0001$ and $P = 0.003$), with non-survivors exhibiting higher concentrations than survivors ($P < 0.05$) [125]. These observations link Cluster 3 to the hyperinflammatory endotype of sepsis, reflecting an early cytokine-driven phase marked by neutrophil and monocyte activation. In addition to their diagnostic value, S100A8/A9 have been shown to propagate inflammation and contribute to later immune dysregulation [126]. Thus, Cluster 3 likely represents an acute inflammatory axis whose elevated activity is associated with early disease severity and poor clinical outcomes.

These modules underscore the multifactorial nature of sepsis. Importantly, the identified module-level signatures should not be interpreted as strictly sequential stages inferred from longitudinal trajectories. Instead, they represent distinct transcriptional programs that may coexist and shift in dominance over the course of illness. This interpretation aligns with contemporary immunological models framing sepsis as a dynamic continuum of overlapping hyperinflammatory and immunosuppressive responses, rather than a linear progression through discrete phases [4, 127]. The modular architecture enhances biological interpretability and offers a framework for immune-state-informed clinical decision-making. Identifying which transcriptional module predominates in an individual patient could help tailor immunomodulatory interventions, such as anti-inflammatory therapy for hyperinflammatory profiles, myeloid-targeted strategies for innate-dominant activation, or immune-stimulatory agents for immunosuppressive endotypes. Such stratification is consistent with emerging precision medicine approaches in sepsis and may inform future adaptive trial designs where treatment allocation is guided by transcriptomic immune profiling rather than syndromic classification alone.

Notably, comparison with clinically established protein biomarkers reveals important insights into the strengths and limitations of transcriptomic versus proteomic diagnostics. Several widely used markers in sepsis diagnosis, including C-reactive protein (CRP, gene: *CRP*) [128], procalcitonin (PCT, gene: *CALCA*) [129], interleukin-6 (IL-6, gene: *IL6*) [130], tumor necrosis factor-alpha (TNF-α, gene: *TNF*) [131], presepsin (soluble CD14 subtype, sCD14-ST, gene: *CD14*) [132], and soluble urokinase plasminogen activator receptor (suPAR, gene: *PLAUR*) [41], were initially included in our 55-gene panel. However, Despite their clinical relevance, these genes did not consistently rank as significant features at the transcriptomic level across the analyzed datasets. This discrepancy highlights a fundamental distinction: while protein biomarkers capture dynamic systemic responses, they are subject to complex post-transcriptional regulation, transient expression kinetics, and context-dependent variability that may obscure their utility in transcriptome-based modeling. Their exclusion from the final 15-gene panel does not diminish their biological importance, but rather reflects the framework's emphasis on

selecting genes with robust and reproducible transcriptional signatures across diverse cohorts. In contrast, the refined transcriptomic panel, anchored by stable and biologically grounded genes such as CD177, ARG1, S100A8/A9/A12, GATA3, and SOCS3, achieved high reproducibility (MCC = 0.93, AUROC = 0.98) and strong cross-cohort stability, supporting its potential as a scalable diagnostic framework. These findings underscore the complementary roles of protein and transcriptomic biomarkers.

Although this study centers on sepsis, the reproducibility-driven framework we present is broadly applicable beyond immune-mediated diseases. A comparable approach has been successfully employed in neuroblastoma to identify prognostic gene signatures from multi-cohort transcriptomic data [17], underscoring its versatility in other complex conditions. The key strengths of the framework including independent within-cohort modeling, cross-cohort consistency filtering, and robustness to variation in biospecimen type, transcriptomic platform, and clinical annotation, make it well-suited for extension to additional biomedical domains, such as oncology, metabolic disease, or neurological disorders. Provided that a biologically relevant candidate gene set and sufficiently annotated cohorts are available, this strategy enables reliable biomarker discovery in the face of clinical and technical heterogeneity. As such, it offers a scalable and adaptable blueprint for transcriptomic signature development across diverse disease contexts.

While this study provides promising insights, several limitations warrant consideration. First, our analysis is based on retrospective transcriptomic datasets drawn from diverse public sources, each encompassing varied patient populations, clinical settings, and measurement platforms. Such heterogeneity including differences in cohort demographics, timing of sample collection, and use of microarray versus RNA-sequencing technologies can introduce confounding effects that may influence gene expression patterns and limit cross-study comparability.

Moreover, detailed clinical metadata were inconsistently reported across datasets. Many cohorts provided only binary sepsis labels without specification of diagnostic criteria (such as Sepsis-2 versus Sepsis-3), and key covariates such as age, sex, illness severity scores (such as SOFA or APACHE), and comorbidities were unavailable in several datasets. This precluded systematic covariate adjustment or stratified analysis across the full cohort landscape. To address this, we independently trained and evaluated models within each dataset and retained genes in the final panel only if they demonstrated reproducible diagnostic utility across multiple independent cohorts.

We also acknowledge variability in sample processing protocols, including the use of whole blood, leukocyte-enriched fractions, or PBMCs, which can affect cellular composition and downstream transcriptomic profiles. Additionally, because the majority of datasets comprised adult patients, the current findings may not generalize to pediatric or neonatal sepsis, which involves distinct immune ontogeny and transcriptional responses. Future studies should include age-specific cohorts with harmonized clinical metadata to assess the applicability of these signatures across diverse patient populations.

Finally, our focus on mRNA-level expression does not fully capture the complexity of protein-level dynamics or functional immune states. Post-transcriptional regulation, protein degradation, and signaling pathway modulation may obscure relationships between gene expression and biological activity. Accordingly, validation of candidate markers at the protein level and integration with complementary modalities such as

proteomics and metabolomics will be critical to fully elucidate the immunopathology of sepsis and support clinical translation.

This study provides a foundation for several promising extensions. First, applying the proposed framework to single-cell RNA sequencing (scRNA-seq) would enable investigation of gene expression at cellular resolution and uncover cell type-specific diagnostic signatures. Such efforts could elucidate the contributions of distinct immune populations to sepsis pathophysiology. To maximize relevance, future studies should prioritize whole-blood or leukocyte-retaining single-cell platforms, since PBMC-based scRNA-seq omits key cell types such as mature neutrophils. Complementary modalities such as CITE-seq or flow cytometry for CD177 protein quantification could further validate these markers in their cellular context.

Second, integrating multi-omics data (including proteomics and metabolomics) may offer a more comprehensive view of host responses, reveal post-transcriptional regulation, and link mRNA (messenger RNA) signatures to actionable protein biomarkers [133]. By linking mRNA signatures to protein-level biomarkers and metabolic alterations, such approaches could enhance biological interpretability and clinical actionability.

From a translational standpoint, the 15-gene panel is technically compatible with targeted multiplex RT-qPCR assays and can be measured from routine whole-blood samples (such as PAXgene-stabilized blood), supporting rapid and cost-effective testing in emergency and intensive-care settings. We further envision prospective clinical validation studies involving early-time-point whole-blood sampling from patients with suspected sepsis, with diagnostic performance evaluated against established clinical criteria such as Sepsis-3 definitions. Optional longitudinal sampling could additionally enable assessment of how modular expression patterns relate to immune-response trajectories and clinical heterogeneity over time.

In terms of modeling strategy, while Random Forest was selected for its robustness and interpretability, future work could incorporate complementary classifiers such as support vector machines, gradient boosting, or deep neural networks. Ensemble learning and meta-modeling frameworks may improve diagnostic accuracy and generalizability. Importantly, leave-one-dataset-out cross-validation (LODO-CV) should be employed to rigorously evaluate model transferability across cohorts, platforms, and clinical settings.

In parallel, scaling this framework to accommodate the increasing size and complexity of transcriptomic data will require parallel computing and advanced machine learning. Distributed architectures such as Apache Spark have demonstrated substantial speedup for large-scale RNA classification tasks [134]. Likewise, interpretable deep learning models, such as convolutional-transformer hybrids [135] and SHAP-enhanced classifiers [136] offer avenues for improving both performance and biological insight. Adapting these tools for transcriptomic biomarker discovery, while leveraging parallelization to manage heterogeneity and computational load, represents a compelling direction for future development.

Finally, prospective clinical studies are essential to validate the 15-gene signature in real-time diagnostic settings and assess its predictive value for clinical outcomes such as severity and mortality. This could involve implementing the panel in point-of-care multiplex assays or transcriptomic diagnostics in emergency and intensive care units. Benchmarking against the FDA-cleared SeptiCyte LAB assay in this study provides an

initial step toward clinical contextualization, although further validation in independent cohorts remains necessary. Pursuing these directions may accelerate clinical translation and support personalized sepsis management.

Abbreviations

AUROC	Area under the receiver operating characteristic curve
BH	Benjamini–Hochberg
CRP	C-reactive protein
DC	Dendritic cell
DAMP	Damage-associated molecular pattern
DEG	Differentially expressed gene
GEO	Gene expression omnibus
GO	Gene ontology
KEGG	Kyoto encyclopedia of genes and genomes
LOFO	Leave-one-feature-out
LPS	Lipopolysaccharide
MA	Microarray
MCL	Markov cluster algorithm
MCC	Matthews correlation coefficient
ML	Machine learning
NK	Natural killer (cell)
PBMC	Peripheral blood mononuclear cell
PCT	Procalcitonin
PPI	Protein–Protein interaction
RF	Random forest
RMA	Robust multi-array average
RNA	Ribonucleic acid
ROC	Receiver operating characteristic
scRNA-seq	Single-cell RNA sequencing
SMOTE	Synthetic minority over-sampling technique
SOCS3	Suppressor of cytokine signaling 3
suPAR	Soluble urokinase plasminogen activator receptor
TLR4	Toll-like receptor 4
TNF-α	Tumor necrosis factor alpha
TPR	True positive rate
TNR	True negative rate
PPV	Positive predictive value
NPV	Negative predictive value
VST	Variance stabilizing transformation

Acknowledgements
The authors thank the reviewers of the CIBB 2025 conference for their feedback.

Author contributions
T.J. performed the dataset search, conducted the computational analyses, and contributed to the writing of the article. D.C. designed and supervised the study, and also contributed to the writing of the article. Both authors approved the current version of the article for publication.

Funding
Open access funding provided by Università degli Studi di Milano - Bicocca within the CRUI-CARE Agreement. The work of D.C. is partially funded by the Italian Ministero Italiano delle Imprese e del Made in Italy under the Digital Intervention in Psychiatric and Psychologist Services (DIPPS) program (project code F/310240/01-04/X56), within the framework "Innovation Agreements" (Accordi per l'Innovazione), and is partially supported by the Ministero dell'Università e della Ricerca of Italy under the "Dipartimenti di Eccellenza 2023–2027" ReGAInS Grant assigned to the Dipartimento di Informatica, Sistemistica e Comunicazione at Università di Milano-Bicocca. The funders had no role in study design, data collection and analysis, decision to publish, or preparation of the manuscript.

Availability of data and materials
All datasets used in this study are publicly available in GEO and their accession codes are listed in Table 2a, b.

Software code availability
Our R software code is openly available under the GPL 3.0 license at https://github.com/TanyaJohary/sepsis-diagnosis.

Declarations

Ethics approval and consent to participate
Ethics approval were collected by each dataset curators in their original studies. Consents to participate from the patients were collected by each dataset curators in their original studies.

Consent for publication
Consents for publication from the patients were collected by each dataset curators in their original studies.

Competing interests
The authors declare no competing interests.

Received: 5 November 2025 / Accepted: 2 February 2026
Published online: 19 February 2026

References

1. Jr JMO, Ali NA, Aberegg SK, Abraham E. Sepsis. Am J Med. 2007;120(12):1012–22. https://doi.org/10.1016/j.amjmed.2007.01.035.
2. Martin GS. Sepsis, severe sepsis, and septic shock: changes in incidence, pathogens, and outcomes. Expert Rev Anti-infect Ther. 2012;10(6):701–6. https://doi.org/10.1586/eri.12.50.
3. Angus DC, Poll T. Severe sepsis and septic shock. N Engl J Med. 2013;369(9):840–51. https://doi.org/10.1056/NEJMra1208623.
4. Hotchkiss RS, Monneret G, Payen D. Sepsis-induced immunosuppression: from cellular dysfunctions to immunotherapy. Nat Rev Immunol. 2013;13(12):862–74. https://doi.org/10.1038/nri3552.
5. Venet F, Monneret G. Advances in the understanding and treatment of sepsis-induced immunosuppression. Nat Rev Nephrol. 2018;14(2):121–37. https://doi.org/10.1038/nrneph.2017.165.
6. Prescott HC, Angus DC. Enhancing recovery from sepsis: a review. JAMA. 2018;319(1):62–75. https://doi.org/10.1001/jama.2017.17687.
7. Iwashyna TJ, Ely EW, Smith DM, Langa KM. Long-term cognitive impairment and functional disability among survivors of severe sepsis. JAMA. 2010;304(16):1787–94. https://doi.org/10.1001/jama.2010.1553.
8. Kumar A, Roberts D, Wood KE, Light B, Parrillo JE, Sharma S, et al. Duration of hypotension before initiation of effective antimicrobial therapy is the critical determinant of survival in human septic shock. Crit Care Med. 2006;34(6):1589–96. https://doi.org/10.1097/01.CCM.0000217961.75225.E9.
9. Duncan CF, Youngstein T, Kirrane MD, Lonsdale DO. Diagnostic challenges in sepsis. Curr Infect Dis Rep. 2021;23(12):22. https://doi.org/10.1007/s11908-021-00765-y.
10. Chenoweth JG, Brandsma J, Striegel DA, Genzor P, Chiyka E, Blair PW, et al. Sepsis endotypes identified by host gene expression across global cohorts. Commun Med. 2024;4(1):120. https://doi.org/10.1038/s43856-024-00542-7.
11. Rashid A, Al-Obeidat F, Kanthimathinathan HK, Benakatti G, Hafez W, Ramaiah R, et al. Advancing sepsis clinical research: harnessing transcriptomics for an omics-based strategy—a comprehensive scoping review. Inf Med Unlocked. 2024;44:101419. https://doi.org/10.1016/j.imu.2023.101419.
12. Wang Y, Wang Z, Yu X, Wang X, Song J, Yu D-J, et al. MORE: a multi-omics data-driven hypergraph integration network for biomedical data classification and biomarker identification. Brief Bioinform. 2024. https://doi.org/10.1093/bib/bbae658.
13. Noor S, AlQahtani SA, Khan S. XGBoost-Liver: an intelligent integrated features approach for classifying liver diseases using ensemble XGBoost training model. Comput Mater Continua. 2025;83(1):1435–50. https://doi.org/10.32604/cmc.2025.061700.
14. Almusallam N, Khan S, Alarfaj FK, Ahmad N. A robust deep learning framework for RNA 5-methyluridine modification prediction using integrated features. BMC Biol. 2025. https://doi.org/10.1186/s12915-025-02433-2.
15. Khan S, Noor S, Awan HH, Iqbal S, AlQahtani SA, Dilshad N, et al. Deep-probind: binding protein prediction with transformer-based deep learning model. BMC Bioinform. 2025;26(1):88. https://doi.org/10.1186/s12859-025-06101-8.
16. Chicco D, Alameer A, Rahmati S, Jurman G. Towards a potential pan-cancer prognostic signature for gene expression based on probesets and ensemble machine learning. BioData Min. 2022;15(1):28. https://doi.org/10.1186/s13040-022-00312-y.
17. Chicco D, Sanavia T, Jurman G. Signature literature review reveals AHCY, DPYSL3, and NME1 as the most recurrent prognostic genes for neuroblastoma. BioData Min. 2023;16(1):7. https://doi.org/10.1186/s13040-023-00325-1.
18. Stelzer G, Rosen N, Plaschkes I, Zimmerman S, Twik M, Fishilevich S, et al. The GeneCards suite: from gene data mining to disease genome sequence analyses. Curr Protoc Bioinform. 2016;54(1):1–30113033. https://doi.org/10.1002/cpbi.5.
19. Kanehisa M, Goto S. KEGG: Kyoto encyclopedia of genes and genomes. Nucleic Acids Res. 2000;28(1):27–30. https://doi.org/10.1093/nar/28.1.27.
20. Ashburner M, Ball CA, Blake JA, Botstein D, Butler H, Cherry JM, et al. Gene Ontology: tool for the unification of biology. Nat Genet. 2000;25(1):25–9. https://doi.org/10.1038/75556.
21. Chicco D, Masseroli M. Software suite for gene and protein annotation prediction and similarity search. IEEE/ACM Trans Comput Biol Bioinform. 2015;12(4):837–43. https://doi.org/10.1109/TCBB.2014.2382127.
22. Pinoli P, Chicco D, Masseroli M. Computational algorithms to predict Gene Ontology annotations. BMC Bioinform. 2015;16(Suppl 6):4. https://doi.org/10.1186/1471-2105-16-S6-S4.
23. Brunialti MKC, Martins PS, Carvalho HBD, Machado FR, Barbosa LM, Salomão R. TLR2, TLR4, CD14, CD11B, and CD11C expressions on monocyte surfaces and cytokine production in patients with sepsis, severe sepsis, and septic shock. Shock. 2006;25(4):351–7. https://doi.org/10.1097/01.shk.0000217815.57727.29.
24. Winkler MS, Rissiek A, Priefler M, Schwedhelm E, Robbe L, Bauer A, et al. Human leucocyte antigen (HLA-DR) gene expression is reduced in sepsis and correlates with impaired TNF-alpha response: a diagnostic tool for immunosuppression? PLoS ONE. 2017;12(8):0182427. https://doi.org/10.1371/journal.pone.0182427.
25. Li Z, Lin L, Kong Y, Feng J, Ren X, Wang Y, et al. Gut microbiota, circulating inflammatory proteins and sepsis: a bi-directional Mendelian randomization study. Front Cell Infect Microbiol. 2024;14:1398756. https://doi.org/10.3389/fcimb.2024.1398756.
26. Xia D, Wang S, Liu A, Li L, Zhou P, Xu S. CCL25 inhibition alleviates sepsis-induced acute lung injury and inflammation. Infect Drug Resist. 2022;15:3309–21. https://doi.org/10.2147/IDR.S352544.
27. Chen W, Guo W, Li Y, Chen M. Integrative analysis of metabolomics and transcriptomics to uncover biomarkers in sepsis. Sci Rep. 2024;14(1):9676. https://doi.org/10.1038/s41598-024-59400-0.

28. Shao Z, Nishimura T, Leung LLK, Morser J. Carboxypeptidase B2 deficiency reveals opposite effects of complement C3a and C5a in a murine polymicrobial sepsis model. J Thromb Haemost. 2015;13(6):1090–102. https://doi.org/10.1111/jth.12956.
29. Pachot A, Cazalis M-A, Venet F, Turrel F, Faudot C, Voirin N, et al. Decreased expression of the fractalkine receptor CX3CR1 on circulating monocytes as a new feature of sepsis-induced immunosuppression. J Immunol. 2008;180(9):6421–9. https://doi.org/10.4049/jimmunol.180.9.6421.
30. Martínez-García JJ, Martínez-Banaclocha H, Angosto-Bazarra D, Torre-Minguela C, Baroja-Mazo A, Alarcón-Vila C, et al. P2X7 receptor induces mitochondrial failure in monocytes and compromises NLRP3 inflammasome activation during sepsis. Nat Commun. 2019;10:2711. https://doi.org/10.1038/s41467-019-10626-x.
31. Porte R, Davoudian S, Asgari F, Parente R, Mantovani A, Garlanda C, et al. The long pentraxin PTX3 as a humoral innate immunity functional player and biomarker of infections and sepsis. Front Immunol. 2019;10:794. https://doi.org/10.3389/fimmu.2019.00794.
32. Renckens R, Roelofs JJTH, Florquin S, de Vos AF, Lijnen HR, van't Veer C, et al. Matrix metalloproteinase-9 deficiency impairs host defense against abdominal sepsis. J Immunol. 2006;176(6):3735–41. https://doi.org/10.4049/jimmunol.176.6.3735.
33. Fang X, Duan S-F, Hu Z-Y, Wang J-J, Qiu L, Wang F, et al. Inhibition of matrix metalloproteinase-8 protects against sepsis serum mediated leukocyte adhesion. Front Med. 2022;9:814890. https://doi.org/10.3389/fmed.2022.814890.
34. Fontaine M, Planel S, Peronnet E, Turrel-Davin F, Piriou V, Pachot A, et al. S100A8/A9 mRNA induction in an ex vivo model of endotoxin tolerance: roles of IL-10 and IFNγ. PLoS ONE. 2014;9(7):100909. https://doi.org/10.1371/journal.pone.0100909.
35. Achouiti A, Föll D, Vogl T, Till JWO, Laterre P-F, Dugernier T, et al. S100A12 and soluble receptor for advanced glycation end products levels during human severe sepsis. Shock. 2013;40(3):188–94. https://doi.org/10.1097/SHK.0b013e31829fbc38.
36. Dimoula A, Pradier O, Kassengera Z, Dalcomune D, Turkan H, Vincent JL. Serial determinations of neutrophil CD64 expression for the diagnosis and monitoring of sepsis in critically ill patients. Clin Infect Dis. 2014;58(6):820–9. https://doi.org/10.1093/cid/cit936.
37. Frimpong A, Owusu EDA, Amponsah JA, Obeng-Aboagye E, Puije W, Frempong AF, et al. Cytokines as potential biomarkers for differential diagnosis of sepsis and other non-septic disease conditions. Front Cell Infect Microbiol. 2022;12:901433. https://doi.org/10.3389/fcimb.2022.901433.
38. KN K, Prakash A, Liu KD, Aouizerat B, Woodruff PG, Erle DJ, et al. Increased expression of neutrophil-related genes in patients with early sepsis-induced ARDS. Am J Physiol Lung Cell Mol Physiol. 2015;308(11):1102–13.
39. Zhang Q, Hu Y, Wei P, Shi L, Shi L, Li J, et al. Identification of hub genes for adult patients with sepsis via RNA sequencing. Sci Rep. 2022;12:5128. https://doi.org/10.1038/s41598-022-09175-z.
40. Siskind S, Brenner M, Wang P. TREM-1 modulation strategies for sepsis. Front Immunol. 2022;13:907387. https://doi.org/10.3389/fimmu.2022.907387.
41. Casagranda I, Vendramin C, Callegari T, Vidali M, Calabresi A, Ferrandu G, et al. Usefulness of suPAR in the risk stratification of patients with sepsis admitted to the emergency department. Intern Emerg Med. 2015;10(6):725–30. https://doi.org/10.1007/s11739-015-1268-7.
42. Bilbault P, Lavaux T, Lahlou A, Uring-Lambert B, Gaub MP, Ratomponirina C, et al. Transient Bcl-2 gene down-expression in circulating mononuclear cells of severe sepsis patients who died despite appropriate intensive care. Intensive Care Med. 2004;30(3):408–15. https://doi.org/10.1007/s00134-003-2118-z.
43. Nakamori Y, Park EJ, Shimaoka M. Immune deregulation in sepsis and septic shock: reversing immune paralysis by targeting PD-1/PD-L1 pathway. Front Immunol. 2021;11:624279. https://doi.org/10.3389/fimmu.2020.624279.
44. Ahmad S, Singh P, Sharma A, Arora S, Shriwash N, Rahmani AH, et al. Transcriptome meta-analysis deciphers a dysregulation in immune response-associated gene signatures during sepsis. Genes. 2019;10(12):1005. https://doi.org/10.3390/genes10121005.
45. Watanabe N, Suzuki Y, Inokuchi S, Inoue S. Sepsis induces incomplete M2 phenotype polarization in peritoneal exudate cells in mice. J Intensive Care. 2016;4:6. https://doi.org/10.1186/s40560-015-0124-1.
46. Weighardt H, Kaiser-Moore S, Schlaukötter S, Rossmann-Bloeck T, Schleicher U, Bogdan C, et al. Type I IFN modulates host defense and late hyperinflammation in septic peritonitis. J Immunol. 2006;177(8):5623–30. https://doi.org/10.4049/jimmunol.177.8.5623.
47. Yoo H, Lee JY, Park J, Yang JH, Suh GY, Jeon K. Association of plasma level of TNF-related apoptosis-inducing ligand with severity and outcome of sepsis. J Clin Med. 2020;9(6):1661. https://doi.org/10.3390/jcm9061661.
48. Gallenstein N, Tichy L, Weigand MA, Schenz J. Notch signaling in acute inflammation and sepsis. Int J Mol Sci. 2023;24(4):3458. https://doi.org/10.3390/ijms24043458.
49. Demaret J, Venet F, Plassais J, Cazalis M-A, Vallin H, Friggeri A, et al. Identification of CD177 as the most dysregulated parameter in a microarray study of purified neutrophils from septic shock patients. Immunol Lett. 2016;178:122–30. https://doi.org/10.1016/j.imlet.2016.08.011.
50. Hao S, Huang M, Xu X, Wang X, Song Y, Jiang W, et al. Identification and validation of a novel mitochondrion-related gene signature for diagnosis and immune infiltration in sepsis. Front Immunol. 2023;14:1196306. https://doi.org/10.3389/fimmu.2023.1196306.
51. Park S, Perumalsamy H, Gerelkhuu Z, Sunderraj S, Lee Y, Yoon TH. Phenotypic landscape of immune cells in sepsis: insights from high-dimensional mass cytometry. ACS Infect Dis. 2024;10(10):2390–402. https://doi.org/10.1021/acsinfecdis.4c00066.
52. Thamm K, Schrimpf C, Retzlaff J, Idowu TO, Meurs M, Zijlstra JG, et al. Molecular regulation of acute Tie2 suppression in sepsis. Crit Care Med. 2018;46(9):928–36. https://doi.org/10.1097/CCM.0000000000003269.
53. Chicco D. geneExpressionFromGEO: an R package to facilitate data reading from Gene Expression Omnibus (GEO). In: Springer protocols, microarray data analysis, vol. 2401. Springer, Berlin, Germany, EU 2021. p. 187–94. https://doi.org/10.1007/978-1-0716-1839-4_12.
54. Baghela A, Pena OM, Lee AH, Baquir B, Falsafi R, An A, et al. Predicting sepsis severity at first clinical presentation: the role of endotypes and mechanistic signatures. eBioMedicine. 2022;75:103776. https://doi.org/10.1016/j.ebiom.2021.103776.
55. Scicluna BP, Klouwenberg PMCK, Vught LA, Wiewel MA, Ong DSY, Zwinderman AH, et al. A molecular biomarker to diagnose community-acquired pneumonia on intensive care unit admission. Am J Respir Crit Care Med. 2015;192(7):826–35. https://doi.org/10.1164/rccm.201502-0355OC.

56. Szakmany T, Fitzgerald E, Garlant HN, Whitehouse T, Molnar T, Shah S, et al. The 'analysis of gene expression and biomarkers for point-of-care decision support in sepsis' study; temporal clinical parameter analysis and validation of early diagnostic biomarker signatures for severe inflammation and sepsis-SIRS discrimination. Front Immunol. 2023;14:1308530. https://doi.org/10.3389/fimmu.2023.1308530.
57. Martínez-Paz P, Aragón-Camino M, Gómez-Sánchez E, Lorenzo-López M, Gómez-Pesquera E, Fadrique-Fuentes A, et al. Distinguishing septic shock from non-septic shock in postsurgical patients using gene expression. J Infect. 2021;83(2):147–55. https://doi.org/10.1016/j.jinf.2021.05.039.
58. Parnell GP, Tang BM, Nalos M, Armstrong NJ, Huang SJ, Booth DR, et al. Identifying key regulatory genes in the whole blood of septic patients to monitor underlying immune dysfunctions. Shock. 2013;40(3):166–74. https://doi.org/10.1097/SHK.0b013e31829ee604.
59. Herwanto V, Tang B, Wang Y, Shojaei M, Nalos M, Shetty A, et al. Blood transcriptome analysis of patients with uncomplicated bacterial infection and sepsis. BMC Res Notes. 2021;14(1):76. https://doi.org/10.1186/s13104-021-05488-w.
60. Cazalis M-A, Lepape A, Venet F, Frager F, Mougin B, Vallin H, et al. Early and dynamic changes in gene expression in septic shock patients: a genome wide approach. Intensive Care Med Exp. 2014;2(1):20. https://doi.org/10.1186/s40635-014-0020-3.
61. Rinchai D, Altman MC, Konza O, Hässler S, Martina F, Toufiq M, et al. Definition of erythroid cell-positive blood transcriptome phenotypes associated with severe respiratory syncytial virus infection. Clin Transl Med. 2020;10(8):244. https://doi.org/10.1002/ctm2.244.
62. Muratsu A, Oda S, Onishi S, Yoshimura J, Matsumoto H, Togami Y, et al. Bacterial sepsis causes more dramatic pathogenetic changes in the Th1 pathway than does viral (COVID-19) sepsis: a prospective observational study of whole blood transcriptomes. Virol J. 2024;21(1):190. https://doi.org/10.1186/s12985-024-02451-6.
63. Sutherland A, Thomas M, Brandon RA, Brandon RB, Lipman J, Tang B, et al. Development and validation of a novel molecular biomarker diagnostic test for the early detection of sepsis. Crit Care. 2011;15(3):149. https://doi.org/10.1186/cc10274.
64. Pankla R, Buddhisa S, Berry M, Blankenship DM, Bancroft GJ, Banchereau J, et al. Genomic transcriptional profiling identifies a candidate blood biomarker signature for the diagnosis of septicemic melioidosis. Genome Biol. 2009;10(11):127. https://doi.org/10.1186/gb-2009-10-11-r127.
65. Linsley PS, Speake C, Whalen E, Chaussabel D. Copy number loss of the interferon gene cluster in melanomas is linked to reduced T cell infiltrate and poor patient prognosis. PLoS ONE. 2014;9(10):109760. https://doi.org/10.1371/journal.pone.0109760.
66. Peña OM, Hancock DG, Lyle NH, Linder A, Russell JA, Xia J, et al. An endotoxin tolerance signature predicts sepsis and organ dysfunction at initial clinical presentation. eBioMedicine. 2014;1(1):64–71. https://doi.org/10.1016/j.ebiom.2014.10.003.
67. Love MI, Huber W, Anders S. Moderated estimation of fold change and dispersion for RNA-seq data with DESeq2. Genome Biol. 2014;15:550. https://doi.org/10.1186/s13059-014-0550-8.
68. Smyth GK. Limma: linear models for microarray data. In: Gentleman R, Carey V, Dudoit S, Irizarry R, Huber W, editors. Bioinformatics and computational biology solutions using R and bioconductor. Springer, New York; 2005. p. 397–420. https://doi.org/10.1007/0-387-29362-0_23.
69. Johnson WE, Li C, Rabinovic A. Adjusting batch effects in microarray expression data using empirical Bayes methods. Biostatistics. 2007;8(1):118–27. https://doi.org/10.1093/biostatistics/kxj037.
70. Chicco D, Oneto L, Tavazzi E. Eleven quick tips for data cleaning and feature engineering. PLoS Comput Biol. 2022;18(12):1010718. https://doi.org/10.1371/journal.pcbi.1010718.
71. Breiman L. Random forests. Mach Learn. 2001;45(1):5–32. https://doi.org/10.1023/A:1010933404324.
72. Chicco D, Jurman G. Survival prediction of patients with sepsis from age, sex, and septic episode number alone. Sci Rep. 2020;10(1):17156. https://doi.org/10.1038/s41598-020-73558-3.
73. Chicco D, Oneto L. Data analytics and clinical feature ranking of medical records of patients with sepsis. BioData Min. 2021;14(1):12. https://doi.org/10.1186/s13040-021-00235-0.
74. Chawla NV, Bowyer KW, Hall LO, Kegelmeyer WP. SMOTE: synthetic minority over-sampling technique. J Artif Intell Res. 2002;16:321–57. https://doi.org/10.1613/jair.953.
75. Mollura M, Chicco D, Paglialonga A, Barbieri R. Identifying prognostic factors for survival in intensive care unit patients with SIRS or sepsis by machine learning analysis on electronic health records. PLOS Digit Health. 2024;3(3):0000459. https://doi.org/10.1371/journal.pdig.0000459.
76. Matthews BW. Comparison of the predicted and observed secondary structure of T4 phage lysozyme. Biochim Biophys Acta. 1975;405(2):442–51. https://doi.org/10.1016/0005-2795(75)90109-9.
77. Chicco D, Jurman G. The Matthews correlation coefficient (MCC) should replace the ROC AUC as the standard metric for assessing binary classification. BioData Min. 2023;16(1):4. https://doi.org/10.1186/s13040-023-00322-4.
78. Chicco D, Jurman G. A statistical comparison between Matthews correlation coefficient (MCC), prevalence threshold, and Fowlkes–Mallows index. J Biomed Inform. 2023;144:104426. https://doi.org/10.1016/j.jbi.2023.104426.
79. Mann HB, Whitney DR. On a test of whether one of two random variables is stochastically larger than the other. Ann Math Stat. 1947;18(1):50–60. https://doi.org/10.1214/aoms/1177730491.
80. Chicco D, Sichenze A, Jurman G. A simple guide to the use of Student's t-test, Mann-Whitney U test, Chi-squared test, and Kruskal-Wallis test in biostatistics. BioData Min. 2025;18(1):56. https://doi.org/10.1186/s13040-025-00465-6.
81. Benjamini Y, Hochberg Y. Controlling the false discovery rate a practical and powerful approach to multiple testing. J R Stat Soc Ser B Methodol. 1995;57(1):289–300. https://doi.org/10.1111/j.2517-6161.1995.tb02031.x.
82. Benjamin DJ, Berger JO, Johannesson M, Nosek BA, Wagenmakers E-J, Berk R, et al. Redefine statistical significance. Nat Hum Behav. 2018;2(1):6–10. https://doi.org/10.1038/s41562-017-0189-z.
83. Cliff N. Dominance statistics: ordinal analyses to answer ordinal questions. Psychol Bull. 1993;114(3):494–509. https://doi.org/10.1037/0033-2909.114.3.494.
84. Spearman C. The proof and measurement of association between two things. Am J Psychol. 1904;15(1):72–101. https://doi.org/10.2307/1412159.
85. Kendall MG. A new measure of rank correlation. Biometrika. 1938;30(1–2):81–93. https://doi.org/10.1093/biomet/30.1-2.81.
86. Efron B. Bootstrap methods: another look at the jackknife. Ann Stat. 1979;7(1):1–26. https://doi.org/10.1214/aos/1176344552.

87. Chen H, Boutros PC. VennDiagram: a package for the generation of highly-customizable Venn and Euler diagrams in R. BMC Bioinform. 2011;12:35. https://doi.org/10.1186/1471-2105-12-35.
88. McHugh L, Seldon TA, Brandon RA, Kirk JT, Rapisarda A, Sutherland AJ, et al. A molecular host response assay to discriminate between sepsis and infection-negative systemic inflammation in critically ill patients: discovery and validation in independent cohorts. PLoS Med. 2015;12(12):1001916. https://doi.org/10.1371/journal.pmed.1001916.
89. Sweeney TE, Shidham A, Wong HR, Khatri P. A comprehensive time-course-based multicohort analysis of sepsis and sterile inflammation reveals a robust diagnostic gene set. Sci Transl Med. 2015;7(287):287–71. https://doi.org/10.1126/scitranslmed.aaa5993.
90. Narasimhan RL, Agarwal R, Sehgal IS. FAIM3:PLAC8 ratio compared with existing biomarkers for diagnosis of severe community-acquired pneumonia: Comparing apples to oranges? Am J Respir Crit Care Med. 2016;193(1):101–2. https://doi.org/10.1164/rccm.201508-1630LE.
91. Szklarczyk D, Gable AL, Lyon D, Junge A, Wyder S, Huerta-Cepas J, et al. STRING v11: protein–protein association networks with increased coverage, supporting functional discovery in genome-wide experimental datasets. Nucleic Acids Res. 2019;47(D1):607–13. https://doi.org/10.1093/nar/gky1131.
92. Enright AJ, Dongen S, Ouzounis CA. An efficient algorithm for large-scale detection of protein families. Nucleic Acids Res. 2002;30(7):1575–84. https://doi.org/10.1093/nar/30.7.1575.
93. Chicco D, Agapito G. Nine quick tips for pathway enrichment analysis. PLoS Comput Biol. 2022;18(8):1010348. https://doi.org/10.1371/journal.pcbi.1010348.
94. Raudvere U, Kolberg L, Kuzmin I, Arak T, Adler P, Peterson H, et al. g:Profiler: a web server for functional enrichment analysis and conversions of gene lists (2019 update). Nucleic Acids Res. 2019;47(W1):191–8. https://doi.org/10.1093/nar/gkz369.
95. Gao Q, Teng Y, Zhu L, Zhang W, Li Z. The immunosuppressive mechanisms induced by sepsis and the corresponding treatment strategies. Front Immunol. 2025;16:1643194. https://doi.org/10.3389/fimmu.2025.1643194.
96. Dave K, Munteanu CR. IL-1R2 as a precision therapeutic target in sepsis: molecular insights into immune regulation. Curr Issues Mol Biol. 2025;47(6):429. https://doi.org/10.3390/cimb47060429.
97. Zanotti S, Kumar A, Kumar A. Cytokine modulation in sepsis and septic shock. Expert Opin Investig Drugs. 2002;11(8):1061–75. https://doi.org/10.1517/13543784.11.8.1061.
98. Carow B, Rottenberg ME. SOCS3, a major regulator of infection and inflammation. Front Immunol. 2014;5:58. https://doi.org/10.3389/fimmu.2014.00058.
99. Grutkoski PS, Chen Y, Chung CS, Ayala A. Sepsis-induced SOCS-3 expression is immunologically restricted to phagocytes. J Leukoc Biol. 2003;74(5):916–22. https://doi.org/10.1189/jlb.0303108.
100. Dai X-K, Ding Z-X, Tan Y-Y, Bao H-R, Wang D-Y, Zhang H. Neutrophils inhibit CD8+ T cells immune response by arginase-1 signaling in patients with sepsis. World J Emerg Med. 2022;13(4):266–73. https://doi.org/10.5847/wjem.j.1920-8642.2022.068.
101. Darcy CJ, Woodberry T, Davis JS, Piera KA, McNeil YR, Chen Y, et al. Increased plasma arginase activity in human sepsis: association with increased circulating neutrophils. Clin Chem Lab Med. 2013;52(4):561–8. https://doi.org/10.1515/cclm-2013-0698.
102. Deng M, Chen S, Wu J, Su L, Xu Z, Jiang C, et al. Exploring the anti-inflammatory and immune regulatory effects of Taohe Chengqi decoction in sepsis-induced lung injury. J Ethnopharmacol. 2024;333:118404. https://doi.org/10.1016/j.jep.2024.118404.
103. Chen Y-J, Lu J-J, Lin C-P, Hu W-C. Microarray analysis reveals sepsis is a syndrome with hyperactivity of TH17 immunity, with over-presentation of the treg cell cytokine TGF-β. Curr Issues Mol Biol. 2025;47(6):435. https://doi.org/10.3390/cimb47060435.
104. Luan Y-Y, Yao Y-M, Xiao X-Z, Sheng Z-Y. Insights into the apoptotic death of immune cells in sepsis. J Interferon Cytokine Res. 2015;35(1):17–22. https://doi.org/10.1089/jir.2014.0069.
105. Du J, Li L, Dou Y, Li P, Chen R, Liu H. Diagnostic utility of neutrophil CD64 as a marker for early-onset sepsis in preterm neonates. PLoS ONE. 2014;9(7):102647. https://doi.org/10.1371/journal.pone.0102647.
106. Corcoran JA, Napier BA. C3aR plays both sides in regulating resistance to bacterial infections. PLoS Pathog. 2022;18(8):1010657. https://doi.org/10.1371/journal.ppat.1010657.
107. Herrero-Cervera A, Soehnlein O, Kenne E. Neutrophils in chronic inflammatory diseases. Cell Mol Immunol. 2022;19:177–91. https://doi.org/10.1038/s41423-021-00832-3.
108. Xia P, Ji X, Yan L, Lian S, Chen Z, Luo Y. Roles of S100A8, S100A9 and S100A12 in infection, inflammation and immunity. Immunology. 2024;171(3):365–76. https://doi.org/10.1111/imm.13722.
109. Wang S, Song R, Wang Z, Jing Z, Wang S, Ma J. S100A8/A9 in inflammation. Front Immunol. 2018;9:1298. https://doi.org/10.3389/fimmu.2018.01298.
110. Parke A, Unge C, Yu D, Sundén-Cullberg J, Strålin K. Plasma calprotectin as an indicator of need of transfer to intensive care in patients with suspected sepsis at the emergency department. BMC Emerg Med. 2023;23:16. https://doi.org/10.1186/s12873-023-00785-y.
111. Broad Institute of MIT and Harvard: Single cell portal. 2024. https://singlecell.broadinstitute.org/single_cell. Accessed 9 Apr 2025.
112. Munoz C, Carlet J, Fitting C, Misset B, Blériot JP, Cavaillon JM. Dysregulation of in vitro cytokine production by monocytes during sepsis. J Clin Invest. 1991;88(5):1747–54. https://doi.org/10.1172/JCI115493.
113. Frydman GH, Ellett F, Jorgensen J, Marand AL, Zukerberg L, Selig MK, et al. Megakaryocytes respond during sepsis and display innate immune cell behaviors. Front Immunol. 2023;14:1083339. https://doi.org/10.3389/fimmu.2023.1083339.
114. Ward NS, Casserly B, Ayala A. The compensatory anti-inflammatory response syndrome (CARS) in critically ill patients. Clin Chest Med. 2008;29(4):617–29. https://doi.org/10.1016/j.ccm.2008.06.010.
115. Silva EE, Skon-Hegg C, Badovinac VP, Griffith TS. The calm after the storm: implications of sepsis immunoparalysis on host immunity. J Immunol. 2023;211(5):711–9. https://doi.org/10.4049/jimmunol.2300171.
116. Uhel F, Azzaoui I, Grégoire M, Pangault C, Dulong J, Tadié J-M, et al. Early expansion of circulating granulocytic myeloid-derived suppressor cells predicts development of nosocomial infections in patients with sepsis. Am J Respir Crit Care Med. 2017;196(3):315–27. https://doi.org/10.1164/rccm.201606-1143OC.
117. Chenoweth JG, Brandsma J, Striegel DA, Genzor P, Chiyka E, Blair PW, et al. Sepsis endotypes identified by host gene expression across global cohorts. Commun Med. 2024;4:120. https://doi.org/10.1038/s43856-024-00542-7.

118. Ton AM, Kox M, Abdo WF, Pickkers P. Precision immunotherapy for sepsis. Front Immunol. 2018;9:1926. https://doi.org/10.3389/fimmu.2018.01926.
119. Fabri A, Kandara K, Coudereau R, Gossez M, Abraham P, Monard C, et al. Characterization of circulating IL-10-producing cells in septic shock patients: a proof of concept study. Front Immunol. 2021;11:615009. https://doi.org/10.3389/fimmu.2020.615009.
120. Lin Z-Q, Chen D, Zhang P-D, Luo J-L, Chen S-Y, Gu S-P, et al. Multi-omics reveal neutrophil heterogeneity in sepsis. Int J Mol Med. 2025;56(6):222. https://doi.org/10.3892/ijmm.2025.5663.
121. Aminov RI, Biryukov SV, Serebryakova MK, Kuzmin DA, Nikonova EY, Kuleshov KV, et al. The analysis of gene expression and biomarkers for point-of-care decision support in sepsis study: temporal clinical parameter analysis and validation of early diagnostic biomarker signatures for severe inflammation and sepsis-sirs. Front Immunol. 2023;14:1308530. https://doi.org/10.3389/fimmu.2023.1308530.
122. Huang J, Xie K, Li H, Wen X, Mei Y, Chen J, et al. Dynamic cd177/cd10 ratio for infection diagnosis and mortality risk stratification in critically ill patients: a prospective cohort study. eBioMedicine. 2025. https://doi.org/10.1016/j.ebiom.2025.106100.
123. Yu N, Liu X, Shi D, Bai L, Niu T, Liu Y. Cd63 and c3ar1: the potential molecular targets in the progression of septic shock. Int J Gen Med. 2022;15:711–28. https://doi.org/10.2147/IJGM.S338486.
124. Sun L, Zhang P, Zhang H, Fan H, Li Y, Zhao Y, et al. Single-cell transcriptomic profiles of peripheral blood immune cells reveal early monocyte and platelet activation in the transition from high-risk states to clinical sepsis. Sci Rep. 2025;15:32879. https://doi.org/10.1038/s41598-025-17078-y.
125. Dubois C, Marcé D, Faivre V, Lukaszewicz A-C, Junot C, Fenaille F, et al. High plasma level of S100A8/S100A9 and S100A12 at admission indicates a higher risk of death in septic shock patients. Sci Rep. 2019;9:15660. https://doi.org/10.1038/s41598-019-52184-8.
126. Wang Q, Long G, Luo H, Zhu X, Han Y, Shang Y, et al. S100A8/A9: an emerging player in sepsis and sepsis-induced organ injury. Biomed Pharmacother. 2023;168:115674. https://doi.org/10.1016/j.biopha.2023.115674.
127. Cao M, Wang G, Xie J. Immune dysregulation in sepsis: experiences, lessons and perspectives. Cell Death Discov. 2023;9(1):465. https://doi.org/10.1038/s41420-023-01766-7.
128. Póvoa P, Almeida E, Moreira P, Fernandes A, Mealha R, Aragão A, et al. C-reactive protein as an indicator of sepsis. Intensive Care Med. 1998;24(10):1052–6. https://doi.org/10.1007/s001340050715.
129. Oliveira CF, Botoni FA, Oliveira CRA, Silva CB, Pereira HA, Nobre V. Procalcitonin versus C-reactive protein for guiding antibiotic therapy in sepsis: a randomized trial. Crit Care Med. 2013;41(10):2336–43. https://doi.org/10.1097/CCM.0b013e31828e969f.
130. Song J, Park DW, Moon S, Cho H-J, Park JH, Seok H, et al. Diagnostic and prognostic value of IL-6, PTX3, and PCT levels among sepsis and septic shock patients: a prospective controlled study according to the Sepsis-3 definitions. BMC Infect Dis. 2019;19:968. https://doi.org/10.1186/s12879-019-4618-7.
131. Gharamti AA, Samara O, Monzon A, Montalbano G, Scherger S, DeSanto K, et al. Proinflammatory cytokines levels in sepsis and healthy volunteers, and tumor necrosis factor-alpha associated sepsis mortality: A systematic review and meta-analysis. Cytokine. 2022;158:156006. https://doi.org/10.1016/j.cyto.2022.156006.
132. Liu B, Chen Y-X, Yin Q, Zhao Y-Z, Li C-S. Diagnostic value and prognostic evaluation of Presepsin for sepsis in an emergency department. Crit Care. 2013;17:244. https://doi.org/10.1186/cc13070.
133. Chicco D, Cumbo F, Angione C. Ten quick tips for avoiding pitfalls in multi-omics data integration analyses. PLoS Comput Biol. 2023;19(7):1011224. https://doi.org/10.1371/journal.pcbi.1011224.
134. Noor S, Awan HH, Hashmi AS, Saeed A, Khan S, AlQahtani SA. Optimizing performance of parallel computing platforms for large-scale genome data analysis. Computing. 2025;107:86. https://doi.org/10.1007/s00607-025-01441-y.
135. Alturki R, Munshi A, Alshawi B, Agarwal K, Khan F, Khan S. CardioBERT: a cardiac identification using fusion features in consumer healthcare. IEEE Trans Consum Electron. 2025;71(2):3522–30. https://doi.org/10.1109/TCE.2025.3575522.
136. Almusallam N, Khan S. Chronic liver disease classification using deep learning with SHAP-optimized hybrid features. iScience. 2025;28(12):113972. https://doi.org/10.1016/j.isci.2025.113972.

Publisher's Note